

AD-A123 982

FINITE DIFFERENCE CALCULATION OF AN INVISCID TRANSONIC
FLOW OVER OSCILLAT..(U) ROYAL AIRCRAFT ESTABLISHMENT
FARNBOROUGH (ENGLAND) T ISHIGURO OCT 80

1/1

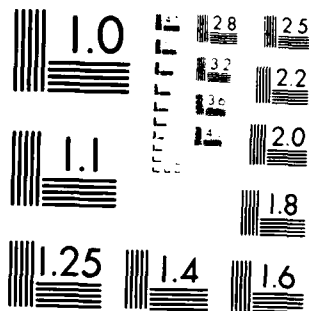
UNCLASSIFIED

RAE-LIBRARY TRANS-2087 DRIC-BR-86199

F/G 20/4

NL

END
DATE
FILED
DTIC



MICROCOPY RESOLUTION TEST CHART
NATIONAL BUREAU OF STANDARDS-1963-A

Trans 2087

ADA 123002

UNLIMITED

Trans 2087

①

DR86177



ROYAL AIRCRAFT ESTABLISHMENT

*

Library Translation 2087

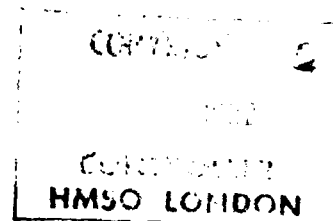
June 1982

FINITE DIFFERENCE CALCULATION OF AN INVISCID TRANSONIC FLOW OVER OSCILLATING AIRFOILS

by

T. Ishiguro

*



Procurement Executive, Ministry of Defence
Farnborough, Hants

DTIC
ELECTE
S **T**
FEB 01 1983
E

DTIC FILE COPY

UNLIMITED 88 01 31 005

Translations in this series are available
from:

THE R.A.E. LIBRARY
Q.4 BUILDING
R.A.E. FARNBOROUGH
HANTS

New translations are announced monthly in:

"LIST OF R.A.E. TECHNICAL REPORTS,
TRANSLATIONS and BIBLIOGRAPHIES"

UNLIMITED

UDC 533.69 : 533.6.013.419 : 533.6.011.35

ROYAL AIRCRAFT ESTABLISHMENT

Library Translation 2087

Received for printing 30 June 1982

FINITE DIFFERENCE CALCULATION OF AN INVISCID TRANSONIC FLOW
OVER OSCILLATING AIRFOILS

by

T. Ishiguro

Japan National Aerospace Laboratory TR-632, October 1980

Translated by
D. Jackson

Translation edited by
Deborah J. Salmond

AUTHOR'S SUMMARY

A procedure is presented to calculate the compressible inviscid unsteady transonic flow over an airfoil, which oscillates sinusoidally in pitch. In order to treat precisely boundary conditions on the oscillating airfoil surface and at infinity, the exterior of the airfoil-shaped contour in the physical plane is mapped onto a rectangle in a computational plane. The two-dimensional unsteady Euler equations are solved there by the Lax-Wendroff finite difference scheme with artificial viscosity. Test calculations were made for the unsteady flows over the Joukowski airfoil and the NACA 0012 airfoil oscillating in pitch, in order to obtain several individual flow patterns. The resulting unsteady pressure distributions, shock wave locations, etc, are presented. Furthermore, the unsteady numerical results obtained by this procedure for the NLR 7301 airfoil and the NACA 64A010 airfoil are compared with the experimental ones by Tijdeman and Davis, respectively.

Accession For	
NTIS GRA&I	<input checked="checked" type="checkbox"/>
DTIC TAB	<input type="checkbox"/>
Unannounced	<input type="checkbox"/>
Justification	
By	
Distribution/	
Availability Codes	
Dist	Avail and/or Special
A	

LIST OF CONTENTS

	<u>Page</u>
1 INTRODUCTION	3
2 SETTING UP THE PROBLEM	5
3 SOLUTION OF FUNDAMENTAL DIFFERENTIAL EQUATIONS	6
3.1 Coordinate system and mesh for calculation	6
3.2 Finite difference method at an interior point	8
3.3 Method of handling boundary conditions	9
4 ROUTINE OF NUMERICAL CALCULATION	11
5 EXAMPLES OF NUMERICAL CALCULATION	13
5.1 Tests on capturing numerical values pertaining to various types of unsteady flow fields	13
5.2 Comparisons of the results of the present method with experiments and other methods of calculation	19
5.3 Required computing time	22
5.4 Deviation from Rankine-Hugoniot relation	22
6 CONCLUSION	23
References	24
Tables 1 to 3	in text
Illustrations	Figures I-IV & 1-9

1 INTRODUCTION

Studies on transonic wings have become active recently for improving transport efficiency, such as in aircraft fuel economy. This study relates to unsteady two-dimensional transonic airfoils which forms part of the above studies. The transonic flow field about an airfoil reacts sensitively to a slight change in boundary conditions. For instance, a change in the angle of attack by about 1° results in changes in shock wave position and airfoil surface pressure distribution, and great changes in air force and moment. It is therefore necessary to clarify such unsteady air force phenomena for commercialising a transonic airfoil section. Examples of means for this purpose are wind tunnel experiments and numerical experiments. Examples of wind tunnel experiments currently carried out are mainly on unsteady boundaries, such as an airfoil oscillating sinusoidally in pitch, an airfoil with a flap oscillating in pitch, and an airfoil with time-varying thickness. There are experimental measurements which have been reported by Tijdeman¹, Davis², and others.

In numerical experiments too, a number of methods of calculation for this flow by differential analog have been proposed. Numerical experiments have been restricted to inviscid flow and the transonic small-disturbance equation or the full potential equation or the Euler equations have been taken as governing flow equations. Ballhaus and Goorjian³ proposed a method of calculation using an alternating direction implicit scheme under a low frequency approximation, and Yu, Seebass and Ballhaus⁴ proposed an improvement on it. These methods can be used only where the unsteady disturbance is small. It is impossible to obtain an accurate solution in the neighbourhood of the leading edge by transferring the condition of tangential flow on the upper and lower surfaces to the mean chord line because of the singularity generated at the nose of the chord line. This trend is particularly acute in the case of a blunt-nosed airfoil. Nevertheless, because of the simplicity in handling the equations and boundary conditions, these procedures are inexpensive and are much quicker than other procedures. It is therefore possible to use them for calculations in a large number of cases with the use of a mean angle of attack, main stream Mach numbers, and airfoil shape, etc, as parameters, and to find the trend of variation in the flow state corresponding to a variation in each parameter. In Japan too, Isogai, *et al*⁵ developed a simple program for a small-disturbance potential equation without the low-frequency approximation. With a view to reducing inaccuracies resulting from the use of this equation, Isogai^{6,7} solved the full potential equation using a semi-implicit time-dependent difference method in a cartesian coordinate system and satisfied the tangential flow condition on the fixed curved surface (henceforth called the 'mean airfoil surface') which coincides with the mean position of the oscillating airfoil instead of the mean chord. Chipman and Jameson⁸ carried out a time-dependent coordinate transformation for a sharp-nosed airfoil, such as a circular-arc airfoil, so as to be able to give the tangential flow condition at the true airfoil position, and solved a full-potential equation in conservation form. However, the range of application of these potential equations is limited to flows which contain only weak shock waves because of their isentropic property. For capturing a discontinuity irrespective of strength, it is necessary to solve the Euler equations. The use of these equations involves a high cost of computation and therefore not many results have been published. However, it is

possible to ascertain the effectiveness of numerical calculation by the above-referred-to two simpler equations by comparison of results with those obtained from the Euler equations. Beam and Warming⁹ used an implicit difference scheme for solving the Euler equations, but good accuracy could not be expected for a blunt-nosed airfoil because the boundary conditions were given at a mean chord position. Magnus and Yoshihara¹⁰⁻¹⁴ gave this condition at a mean position on an oscillating airfoil surface, and Lerat and Sides^{15,16} gave the same condition on a true airfoil surface by a time-dependent coordinate transformation and sought the solution with the use of an explicit difference scheme. For a perfect prediction of air forces, the hypothesis of inviscidity should be removed, in order to enable the handling of such viscous phenomena as interaction between an unsteady shock wave and boundary layer, etc. For this purpose, Magnus and Yoshihara¹³ used a method of approximating the displacement effect of a boundary layer, but the possibility of calculations based on the Navier-Stokes equations, which incorporates a viscous flow model, is possible. The calculation tried out by Chyu and Davis¹⁷ for bypassing the current high cost of computation has too coarse a grid spacing. Satisfactory calculations are likely to be made when the cost comes down.

This study proposes a method of calculation for a flow about an airfoil which oscillates sinusoidally in pitch, using the unsteady Euler equations. This method is a variation of the method of calculation for steady flow proposed earlier^{18,19} by the author, by improving the mapping function for grid construction, in order to improve calculation efficiency, and by extending it to enable the handling of unsteady boundary conditions. It will be assumed that the amplitude of pitching is small, and that the boundary conditions are given at the mean airfoil surface position. Magnus and Yoshihara¹² carried out calculations in a finite plane exterior to the mean airfoil surface and superposed several types of Cartesian grids varying in spacing on a physical plane with a curvilinear grid near the airfoil surface. The difference scheme used was an explicit two-step finite difference scheme of the Lax-Wendroff type. In this paper, the following approaches, which differ from the above, are tried out²⁰.

First, the infinite plane exterior to the mean airfoil surface is mapped on to a rectangle to form a computational plane, in order to facilitate the handling of airfoil surface boundary conditions and infinity conditions. On the computational plane, only one uniform grid is spanned. In the vicinity of a shock wave, a fine and uniform grid is superposed when required. Numerical solution of the unsteady Euler equations at a mesh point will be obtained from an application of the time-split Lax-Wendroff scheme, with an artificial viscosity term.

A program will then be made using this method of calculation, and an examination will be made of the possibility of obtaining several types of unsteady flow patterns by using a Joukowski airfoil and the NACA 0012 airfoil. Then, numerical solutions for the NLR 7301 airfoil and the NACA 64A010 airfoil also will be obtained. They will be compared with the results obtained by Tijdeman and Davis.

2 SETTING UP THE PROBLEM

The Euler equations of unsteady two-dimensional flow are used as fundamental differential equations and can be represented in the following conservative form on a physical plane x - y . This equation has previously been non-dimensionalised¹⁸ in reference by main stream density and velocity, and chord length.

$$\begin{pmatrix} \rho \\ \rho u \\ \rho v \\ e \end{pmatrix}_t + \begin{pmatrix} -u \\ \rho u^2 + p \\ \rho uv \\ u(e+p) \end{pmatrix}_x + \begin{pmatrix} -v \\ \rho uv \\ \rho v^2 + p \\ v(e+p) \end{pmatrix}_y = 0 ,$$

$$p \equiv (\gamma - 1) \left\{ e - \rho(u^2 + v^2)/2 \right\} ; \quad (1)$$

a relation $c = \sqrt{(\gamma p)/\rho}$ holds; where t = time, x, y rectangular cartesian coordinates, ρ = density, u = velocity component in x -direction, v = velocity component in y -direction, e = total energy per unit volume, p = pressure, c = speed of sound, γ = specific heat ratio of perfect gas (presumed to be 1.4).

The vector representation of equation (1) is

$$W_t + F_x(W) + G_y(W) = 0 \quad (2)$$

where $W = \begin{pmatrix} \rho \\ \rho u \\ \rho v \\ e \end{pmatrix} .$

The problem of determining an inviscid flow around an unsteady airfoil can be replaced numerically by the problem of solving equation (2) subject to the following three boundary conditions.

(1) Tangential flow condition - the flow velocity vector is tangent to the unsteady airfoil surface.

(2) Condition of the trailing edge - the Kutta-Joukowski condition (the pressures on the upper and lower surfaces at the trailing edge are identical) in the absence of a shock wave at the trailing edge and the Rankine-Hugoniot relation holds in the presence of a shock wave at the trailing edge.

(3) Infinity conditions - at upstream infinity, conditions are free stream conditions, that is $W = W_\infty$ (hereinafter the subscript ∞ will be used for indicating the free stream), where $\rho_\infty = 1$, $u_\infty = \cos \alpha_0$, $v_\infty = \sin \alpha_0$, $p_\infty = 1/(\gamma M_\infty^2)$ where α_0 is the mean angle of attack.

At downstream infinity and the main stream subsonic, shock wave can be divided into downwash and the rest, then $p = p_\infty$, $\vec{U} \propto \vec{z}_\infty$, $(\partial U / \partial z_\infty) = 0$, $(\partial p / \partial z_\infty) = 0$ (\vec{z}_∞ = direction of the main stream; \vec{U} = velocity spectrum) hold for the former and the flow in the rest is the main stream. Where the main stream is supersonic, the downstream solution depends upon the upstream values, thus no conditions are necessary.

In this study, the problem of unsteadiness will be confined to the flow about an airfoil oscillating sinusoidally in pitch with small amplitude, and the conditions of tangential flow will be applied at the mean position of the oscillating airfoil. The method of calculation using a computer for solving this problem will be discussed in the next section.

3 SOLUTION OF FUNDAMENTAL DIFFERENTIAL EQUATIONS

3.1 Coordinate system and mesh for calculation

In order to facilitate the insertion of the condition of tangential flow at the airfoil surface and the condition at infinity, the mean airfoil surface and its exterior on a physical plane (x, y) will be mapped on to a rectangle and its interior on a computational plane (ξ, η) . This mapping is carried out with the following three coordinate transformations, which are illustrated in Fig I. The description of mappings (1) and (2) is brief because they have been described in detail in Ref 13 (pp 3,4).

(1) A point on an airfoil surface at the greatest distance from the trailing edge of a mean airfoil surface is called the leading edge, which is selected as the origin. A straight line connecting this with the trailing edge is the x-axis (a closed trailing edge alone is considered). A mean airfoil surface having a trailing edge angle ϵ and its exterior on its physical plane ($z = x - iy$) is conformally mapped on to a unit circle and its exterior on o ($= re^{i\omega}$).

(2) This unit circle and its exterior are conformally mapped on to the lower half of w ($= x' + iy'$) plane.

(3) By using the following function, this lower half plane is mapped on to a rectangle and its interior on the computational plane $\zeta = \xi + i\eta$.

$$\begin{aligned} x' &= \xi g(\xi^2) / (\xi^2 - 4) & (|\xi| \leq 2) \\ y' &= \eta / (1 - \eta) & (0 \leq \eta \leq 1) \end{aligned}$$

In the above equation, g is a polynomial, and its coefficient should be fixed accurately by a method described later, to obtain a highly efficient calculation of flow pattern which can be visualised in each case before starting the calculation of flow patterns.

In Fig I, the wavy line and broken line show the curve to which the three straight lines $\xi = \pm b$, $\eta = c$ correspond on each coordinate plane.

With this series of mappings, the mean airfoil surface is made to correspond to the section ($\eta = 0$, $-a \leq \xi \leq a$), upstream infinity to the upper side of the rectangle, and

downstream infinity to both lateral sides of the rectangle. Thus, all boundary conditions can be given on the four sides of the rectangle. The domain for computation is this rectangle and its interior.

The Euler equations (2) on the physical plane are transformed into the following on the computational plane.

$$W_t + F_\xi(W)\xi_x + G_\xi(W)\xi_y + F_\eta(W)\eta_x + G_\eta(W)\eta_y = 0. \quad (3)$$

Differential coefficients ξ_x, ξ_y, η_x and η_y can be determined for each mapping function, using a chain rule (Ref 18, p.4). For solving equation (3) by a finite difference method, first place a uniform Cartesian grid system having widths $\Delta\xi$ and $\Delta\eta$ on the computational plane to make lattice lines coincide with the four sides of the rectangle, and represent the lattice points by symbols (i,j) . The grid image on the corresponding physical plane is also orthogonal. As will be shown later in examples, the j group of lattice lines are higher in density as they approach the airfoil surface, whereas the density distribution among the i group of lattice lines is designed to be adjustable by means of the function g in the mapping in equation (3). Taking into consideration the pattern of a predicted flow, g is fixed to make the grid image density on the physical plane higher in an area where flow variation is great (in the vicinity of shock wave, leading edge and trailing edge). However, arbitrary points ξ_1 and $-\xi_1$ on the ξ -axis downstream of the trailing edge must correspond to the same point. The function g is made a function of ξ^2 . Because of this, the lattice distributions on the upper and lower surfaces of an airfoil are similar in shape. However, where the flow patterns on the upper and lower surfaces differ considerably, for instance, in the presence of a shock wave only on the upper surface, the grid in its vicinity must be made fine, but there is no need to do this on the lower surface. For maintaining computational efficiency in such a case, a grid (width $\Delta\xi$) was formed on first fixing g to match the flow pattern on the lower surface, and a finer grid (width $\Delta\xi/4$) was superposed on that part of the grid system corresponding to the vicinity of the shock wave on the upper surface. An automatic superposition of that section with the $1/4$ -width grid was possible by the inclusion of a routine for designating (i_1, i_2) . With the selection of a suitable g , and the superposition of the $1/4$ -width grid, an improvement in computational efficiency and an accurate numerical grasping of flow pattern variation were made possible.

Because the boundary conditions of an oscillating airfoil are applied at the mean position of the airfoil surface a time-dependent grid system is not required.

The definition of g : The correspondence between $z = x - iy$ and $w = x' + iy'$ is obtainable from mappings (1) and (2), therefore we will try to obtain a curve (inclusive of a mean airfoil surface) corresponding to the x' -axis. Choose a suitable number of points (x_ℓ, y_ℓ) , where $\ell = 1, 2, 3, \dots, L$, on that curve and arrange the desired lattice-point subscript i_ℓ for each of these, while taking into consideration the predicted flow pattern. Then, find x'_ℓ corresponding to (x_ℓ, y_ℓ) and approximate L sets of data $\left[\xi_\ell^2, \left(\xi_\ell^2 - 4 \right) x'_\ell / \xi_\ell \right]$, which can be calculated from x'_ℓ and $\xi_\ell = (i_\ell - 1)\Delta\xi$,

with a number of least squares polynomials differing in degree. Draw a grid image for each degree on the physical plane, select one which is likely to be suitable for flow calculation, and define g as follows.

$$g(\xi^2) \equiv (\xi^2 - 4)x'/\xi = \sum_{m=0}^M C_m \xi^{2m}.$$

3.2 Finite difference method at an interior point¹⁸

The solution by finite differences for W at the point (i,j) , after N time steps is represented by $W_{i,j}^N$. For mesh points in the rectangle, the following time-split difference approximations are applied to equation (3) (Fig II).

$$W_{i,j}^{N+1} = L_\xi L_\eta W_{i,j}^N, \quad W_{i,j}^{N+2} = V_\xi V_\eta L_\xi L_\eta W_{i,j}^{N+1}.$$

The differential operator L_ξ in the above equations is a two-step Lax-Wendroff operator of second order accuracy.

$$L_\xi W_{i,j} \equiv W_{i,j} - \frac{\Delta t}{\Delta \xi} \left\{ (\tilde{F}_{i+\frac{1}{2},j} - \tilde{F}_{i-\frac{1}{2},j}) \xi_{x_{i,j}} + (\tilde{G}_{i+\frac{1}{2},j} - \tilde{G}_{i-\frac{1}{2},j}) \xi_{y_{i,j}} \right\},$$

$$\tilde{W}_{i+\frac{1}{2},j} \equiv \frac{1}{2}(W_{i+1,j} + W_{i,j}) - \frac{\Delta t}{2\Delta \xi} \left\{ (F_{i+1,j} - F_{i,j}) \xi_{x_{i+\frac{1}{2},j}} + (G_{i+1,j} - G_{i,j}) \xi_{y_{i+\frac{1}{2},j}} \right\}.$$

L_η can be defined similarly. The von Neumann condition for $L_\xi L_\eta L_\xi L_\eta$ can be given¹⁸ by the following equation

$$\Delta t \leq \min \left(\frac{\Delta \xi}{|u \xi_x + v \xi_y| + c}, \frac{\Delta \eta}{|u \eta_x + v \eta_y| + c} \right) \equiv \Delta T.$$

For obtaining a value for the magnitude of time-step for use in actual calculations, multiply ΔT by a suitable scalar $C_{\Delta t}$ (less than 1), so that the stability criterion is satisfied. The artificial viscosity operator V_ξ can be defined as follows:

$$V_\xi W_{i,j} \equiv W_{i,j} + \lambda_\xi \left\{ |U_{i+1,j}^\xi - U_{i,j}^\xi| (W_{i+1,j} - W_{i,j}) - |U_{i,j}^\xi - U_{i-1,j}^\xi| (W_{i,j} - W_{i-1,j}) \right\},$$

$$U^\xi \equiv u \xi_x + v \xi_y.$$

V_η is defined similarly. The quantities λ_ξ and λ_η are suitably chosen to ensure the numerical stability of the solution with artificial viscosity terms.

3.3 Method of handling boundary conditions

As was said in section 3.1, the whole of the airfoil surface, trailing edge, and infinities correspond to the four sides of the rectangle on the computational plane. Thus a method for obtaining numerical solutions which satisfy the boundary conditions discussed in section 2 will be described.

(1) Two sections ($a < \xi < 2$ and $-a > \xi > -2$) on the base ($\eta = 0$): They correspond to the same curve, which is not a boundary, on the physical plane in Fig I (the wavy-line sections in Fig II). Thus the method relating to the internal point discussed in section 3.2 will be applied with the relation $W(\xi) = W(-\xi)$ assumed to hold.

(2) Section $|\xi| < a$ on the base ($\eta = 0$): This corresponds to mean airfoil surface. The condition of sinusoidal oscillation of the solid airfoil surface must be satisfied. In other words, the velocity component of a flow normal to the airfoil surface must equal the component of velocity of the surface in the same direction. W on the airfoil surface in this calculation is obtainable from the following representation ($j = 1$ indicates the base).

$$W_{i,1}^{N+1} = O \hat{L}_\eta L_\xi W_{i,1}^N, \quad W_{i,1}^{N+2} = O V_\xi L_\xi \hat{L}_\eta W_{i,1}^{N+1}.$$

In the above equation, \hat{L}_η can be defined as $\hat{L}_\eta W_{i,1} = h(\hat{L}_\eta W_{i,2}, \hat{L}_\eta W_{i,3})$ where h is an extrapolation function relating to the distance between corresponding points on the physical plane of grid points $j = 1, 2, 3$. First, the intermediate quantity \hat{W} will be obtained from the following equation:

$$\hat{W}_{i,1}^{N+1} = \hat{L}_\eta L_\xi W_{i,1}^N, \quad \hat{W}_{i,1}^{N+2} = V_\xi L_\xi \hat{L}_\eta W_{i,1}^{N+1}.$$

The velocity components in \hat{W} are replaced by the tangential component, \hat{v}_{\tan} and the normal component \hat{v}_{nor} at that time. This quantity \hat{W} can be updated¹⁴ to W by an oscillation operator O which is used in many operations to be discussed later.

We will now consider (Fig III) a coordinate system $X - Y$ ($X =$ direction of the airfoil) which is fixed to the moving airfoil, in addition to coordinate system $x - y$, on the physical plane. When the airfoil is in its mean attitude, they coincide with each other. Let us assume that an airfoil is oscillating sinusoidally in pitch about a central axis of coordinates $(x_c, y_c) = (X_c, Y_c)$, with

$$\alpha(t) = \alpha_0 + \beta(t), \quad \beta(t) = \Delta\alpha \sin 2kt.$$

where $\alpha(t) =$ angle of attack, $\alpha_0 =$ mean angle of attack, $\beta(t) =$ angle of pitching, $\Delta\alpha =$ amplitude of pitching, $k =$ frequency parameter.

The frequency parameter k is defined by

$$k = \frac{1}{2} C_{\omega}' / U_{\infty}$$

where C = airfoil chord length, ω' = angular frequency, and U_{∞} = speed of main stream.

The position of point m (coordinates (X_m, Y_m)) corresponding to a grid fixed to a moving airfoil in the x - y system at the time t is obtainable from the equations

$$x_m(t) = X_c + (X_m - X_c) \cos \varphi(t) + (Y_m - Y_c) \sin \varphi(t)$$

$$y_m(t) = Y_c - (X_m - X_c) \sin \varphi(t) + (Y_m - Y_c) \cos \varphi(t)$$

The velocity component in the outward normal direction at point m on the airfoil is obtainable from the velocity components (\dot{x}_m, \dot{y}_m) in the Cartesian system by means of the equation

$$v_{\text{nor}} = -\dot{x}_m \sin(\varphi_m - \varphi) + \dot{y}_m \cos(\varphi_m - \varphi)$$

where φ_m is the angle between the tangent to the airfoil surface and the airfoil chord measured positive in the clockwise direction. The velocity component \hat{v}_{nor} in a direction normal to the airfoil surface at the time t , which has been obtained earlier, is adjusted to agree with the velocity component v_{nor} of a plane isentropic wave which propagates in the normal direction on the outside of the airfoil. This adjustment causes variation in density and pressure, but it does not change the tangential component of velocity \hat{v}_{tan} . The adjusted density, pressure and flow velocity $(\hat{v}_{\text{tan}}, v_{\text{nor}})$ are used for updating W .

(3) Two points ($\xi = \pm a, \eta = 0$) on the base: These points correspond to the same point, the trailing edge, on the physical plane. Although the conditions differ according to the presence or absence of a shock wave at the trailing edge, as was said earlier, a discontinuous surface is handled as a continuous surface with a steep slope in the finite difference method. Thus, for convenience, in the presence of a mesh point at the trailing edge, numerical solutions for the upper and lower surfaces are obtained and these are then averaged. In the absence of such a mesh point, use the method relating to the internal point discussed in the previous section at two mesh points ($\xi = \pm \xi_T, \eta = 0$) nearest to the base of the rectangle and average their numerical solutions.

(4) ($|\xi| \leq 2, \eta = 1$) on the top side: This corresponds to upstream at infinity, thus it always gives main stream W_{∞} .

(5) ($|\xi| \leq 2, 0 < \eta < 1$) on two lateral sides: This corresponds to downstream at infinity. Where the main stream is supersonic, the numerical solution at a neighbouring grid point within the rectangle is used at the boundary point. In other words, extrapolation with zero-order precision is carried out. On the other hand, if the main stream is subsonic, the condition at infinity discussed in section (3) should be imposed. However it is difficult to use that condition in the present calculation, so the following numerical approximation is made. Whether or not a grid point (IE, j) at $\xi = \pm 2$ is downstream of a shock wave is determined (Fig IV) by whether the value of entropy S_{IB}

of the neighbouring mesh point upstream of $(1B,j)$ is greater than the entropy S_{1B} of the oncoming flow. If $S_{1B} = S_{1E}$ it is presumed that the point is downstream of a shock wave.

If $S_{1B,j}^N > S_{1E}$, then $W_{1E,j}^N = W_{1B,j}^N$ (triangle-marked sections in Fig. 15).

If $S_{1B,j}^N < S_{1E}$, then $P_{1E,j}^N = P_{1B,j}^N$, $\rho_{1E,j}^N = \rho_{1B,j}^N$, $u_{1E,j}^N = u_{1B,j}^N \cos \alpha_0$,
 $v_{1E,j}^N = u_{1B,j}^N \sin \alpha_0$ (broken-line sections in Fig. 15).

4. ROUTINE OF NUMERICAL CALCULATION

Program 'MESH' for forming a mesh with the solutions discussed in the previous chapter, program 'FLOW' for finding a flow about an airfoil by the finite difference method, and program 'RESULT' processing results based on W , with graphs, etc, were prepared. These programs were written in the code for a FACOM 230-75 computer with an array processor unit.

The calculation of the case of an airfoil in a main stream of given Mach number M_∞ oscillating in pitch with angle of attack $\alpha(t) = \alpha_0 + \Delta\alpha \sin 2\pi kt$ about the central axis (X_c, Y_c) was carried out in the following sequence of steps.

- (1) Preparation of the mesh: The function g was determined with program MESH by the procedure discussed in section 3.1. It was decided whether to superpose the W -flow grid and if so the position at which the superposition was to be made was determined.
- (2) Calculation of a steady flow which becomes a starting solution in the calculation of unsteady flow: An unsteady flow about an airfoil placed at an angle of attack α_0 in a main stream of Mach number M_∞ was found by the following procedure. Seek asymptotically steady solution by applying the program FLOW on a suitable starting value with amplitude $\Delta\alpha = 0$. (Described in detail in Ref 18.)
- (3) Calculation of a quasi-steady flow: Although not always necessary, it is advisable to have, before starting the calculation for an unsteady flow ($k \neq 0$), a calculation for the corresponding quasi-steady flow ($k = 0$, oscillation is infinitely slow) for reference. That is, asymptotically steady solutions W are calculated for both maximum angle of attack $(\alpha_0 + \Delta\alpha)$ and minimum angle of attack $(\alpha_0 - \Delta\alpha)$ of the oscillation, as in (2) above. Convergence is obtainable more rapidly from using a starting solution obtained by the method discussed in (2). It is necessary at this time point to examine whether a mesh prepared in (1) is suitable for calculations in (2) and (3). If unsuitable, repeat the preparation in accordance with (1). If the mesh has been found suitable for calculations in (2) and (3), the calculations of the unsteady flow having an angle of attack $\alpha(t)$ continually varying between the above two limits can probably be made satisfactorily.
- (4) Processing the results of the quasi-steady flow calculation: Derive the following from the results of calculations in (2) and (3), using RESULT.

(a) Prepare isobaric charts with sonic lines for three steady flows (angles of attack $\alpha_0 + \Delta\alpha$, α_0 , $\alpha_0 - \Delta\alpha$) and diagrams $[C_p \equiv 2(p - 1/(\gamma M^2))]$ of variation in airfoil surface pressure coefficient C_p with chord length. Integrate C_p to obtain the coefficient of drag C_D , the coefficient of lift C_L , and the moment coefficient C_M .

(b) A diagram of variation in quasi-steady pressure coefficient ΔC_p (or ΔC_p) with chord length, where

$$\Delta C_p \equiv (C_p(\alpha_0 - \Delta\alpha) - C_p(\alpha_0 + \Delta\alpha)) / (2\Delta\alpha) ,$$

or, in the case of a symmetrical airfoil, where $\alpha_0 = 0$:

$$\Delta C_p \equiv (C_p(\alpha_0) - C_p(\alpha_0 + \Delta\alpha)) / \Delta\alpha .$$

(5) Calculations for unsteady flow: With the flow for the mean angle of attack obtained in (2) above, taken as starting solution at $t = 0$, an unsteady flow about an airfoil oscillating sinusoidally in pitch will be obtained with the use of FLOW. Continue calculations until periodic solutions are obtained (about four periods are necessary for coinciding isobaric charts for all periods). During that time, solutions W obtained for equidistant phase angles (every 10° here) were stored in a disc pack to be used later for processing the following results.

(6) Processing of results pertaining to unsteady flow: RESULT was used for deriving the following from the results W stored in (5) above.

(a) Isobaric charts with sonic lines at a series of specified phases, and diagrams of variation in airfoil surface pressure coefficient with chord length.

(b) Unsteady pressure distribution diagram (depiction of first harmonic variation of C_p). That is, to obtain C_{p_i} at a lattice point on an airfoil surface in every equidistant phase angle (10°) from the solution W for the final period stored in (5), and then approximate the data (37 in number) for the period under consideration by a spline interpolation and a fast Fourier transform to get the equation

$$\begin{aligned} C_{p_i}(t) &\sim B_{0_i} + \Delta\alpha \left\{ \text{Re}(C_{p_i}) \sin 2kt + \text{Im}(C_{p_i}) \cos 2kt \right\} \\ &= B_{0_i} + \Delta\alpha | \Delta C_{p_i} | \sin(2kt + \phi_i) . \end{aligned}$$

In the above equation, $\text{Re}(C_p)$ is the real part of unsteady pressure distribution which is of the same phase as the movement of airfoil, and $\text{Im}(C_p)$ is the imaginary part of the unsteady pressure distribution which is in a quadrature with the motion. Further, $| \Delta C_p |$ is the magnitude of the first harmonic and ϕ is phase relative to the airfoil motion. Variation of these four quantities with chord length is shown in a figure.

(c) Air force coefficient and Fourier analysis of the position of the shock wave. The position of the shock wave (X of minimum C_p) was calculated from C_p obtained during the calculation in (b) above. Tangential force coefficient (C_x), normal force

coefficient (C_y), pitching moment coefficient C_M [(X_c, Y_c) centre and positive nose-up] were calculated for each phase angle (10°) by integration. Then, each of these was represented by f and the data (37 in number) thus obtained for one period were approximated by the following equation, obtained by spline interpolation and fast Fourier transform. Numerical values of B_0 , A_n and ϕ_n were obtained

$$f(t) = B_0 + \sum_{n=1}^{N'} \{A_n \sin(2n\pi kt + \phi_n)\}.$$

If the magnitude of the second and subsequent harmonics, A_n , where $n = 2, 3, \dots$, is smaller than that of the first harmonic A_1 , f changes sinusoidally with respect to time. In other words, it can be said that a linear relation exists between the displacement of an airfoil and its f . Where this is not so, these coefficients serve as an indicator of the degree of deviation from the sinusoidal form.

5 EXAMPLES OF NUMERICAL CALCULATION

Let us illustrate the numerical capturing of various types of unsteady shock wave phenomena at various main stream Mach numbers, by the calculation sequence given in steps 1 to 5. Experimental conditions differ slightly from the conditions of calculation used here because of the effects of interference by wind tunnel walls and viscosity, but cases 6 and 7 illustrate the reproduction by calculation of an analogous flow pattern which enables a comparison with the experiments of Tijdeman to be made. In case 8, the present method of calculation are compared with the results of Davis' experiments, and of other methods of calculation.

The types of airfoil, the values of parameters (main stream Mach number, mean angle of attack, amplitude of pitching, reduced frequency, position of central axis of oscillation, number of mesh points, coefficient of time-step and coefficient of artificial viscosity), the presence or absence of superposition with $\Delta x/4$ -wide mesh, and numbers of mesh images used in the calculation in each are shown collectively in Table 1. The numbers of the figures showing the results of the principal calculations in all cases are given in Table 2. The symbols () indicate the numbers of the figures showing comparable results obtained by experiments or other methods of calculation. All figures pertain to a period a number of cycles $2\pi/2\pi$ from $t = 0$ have occurred. The characteristics and results of the calculations will now be examined case by case.

5.1 Tests on capturing numerical values pertaining to various types of unsteady flow fields

(Case 1) Numerical values pertaining to unsteady phenomena involving the generation, growth and annihilation of a weak shock wave

At the free stream Mach number of 0.73, a steady flow produced by the symmetrical airfoil NACA 0012 does not contain a shock wave when the angle of attack is 0° , as is shown in Fig 1-2f, but it does when the angle of attack is 2° . Under the conditions of a mean angle of attack 0° and amplitude of pitching 2° , calculations at $k = 0.1$ were made. The development of the flow was followed numerically, through the generation of a

Table 1
Values of parameters and of grids used in calculations

Case	Airfoil	Main stream Mach No. M_∞	Mean angle of attack α_0	Amplitude of pitching $\Delta\alpha$	Damped frequency $k = \frac{\omega C}{2U}$	Position of central axis of oscillation (X_c, Y_c)	No. of lattice points	$\Delta x/4$ -wide mesh overlay	Mesh image on physical plane	Coefficient of time division C_{dt}	Coefficient of artificial viscosity $\nu_{\text{art}} = \lambda$
1	NACA 0012	0.73	0°	2°	0.1	(0.5, 0)	(120 × 31)	no	Fig 1-1	0.2	0.1
2	Joukowski	0.72	2°	2°	0.1 0.25	(0.5, 0)	(101 × 31)	yes	Fig 2-1	0.2	0.02 0.03
3	Joukowski	0.92	0°	3°	0.1	(0.5, 0)	(121 × 31)	no	Fig 3-1	0.2	0.15
4	Joukowski	0.93	0°	3°	0.1	(0.5, 0)	(121 × 31)	no	Fig 3-1	0.3	0.15
5	Joukowski	1.4	0°	5°	0.1	(0.5, 0)	(121 × 31)	no	Fig 3-1	0.2	0.2
6	NLR 7301	0.7	1.5°	0.5°	0.192	(0.4, -1/60)	(101 × 31)	yes	Fig 6-1	0.2	0.03
7	NLR 7301	0.721	-0.19°	0.5°	0.181	(0.4, -1/60)	(81 × 31)	no	Fig 7-1	0.2	0.05
8	NACA 64A010	0.8	0°	1°	0.2	(0.25, 0)	(120 × 31)	yes	Fig 8-1	0.14	0.01

Table 2
Numbers of figures showing results of calculation in each case

Content of figure		Case numbers							
		1	2	3	4	5	6	7	8
Steady flow Angle of attack $\alpha_0, \alpha_0 \pm \Delta\alpha$	Isobaric chart $X - C_p$	*1-2f 1-3a	2-2 2-5a	3-2 3-4a	4-1 4-3a	5-1 5-3a	6-2 (6-4)	7-2 (7-4)	8-2 8-4 (8-5)
	Quasi-steady flow $X - \Delta C_p$	1-4	2-6	3-5	4-4	5-4	(6-5)	(7-5)	(8-6)
Unsteady flow $\alpha(t) = \alpha_0 + \Delta\alpha \sin 2kt$	Isobaric chart $X - C_p$	1-2a~e 1-3b	2-3 2-4 2-5b, c	3-3 3-4b	4-2 4-3b	5-2 5-3b	6-3 6-4c	7-3 7-4c	8-3 8-4
	$X - \text{Re}(C_p)$ $\text{Im}(C_p)$	1-5	2-7	3-6	4-5	5-5	(6-6) (6-7)	(7-6) (7-8)	(8-7)
Solution for period	$X - C_p $ ϕ	1-6	2-8	3-7	4-6	5-6	(6-8)	(7-7) (7-9)	(8-8)

* All numbers refer to figures

() Result of comparing the present method with experiment or other calculation method.

shock wave, its growth and decay on the upper surface, followed by the same events on the lower surface in every period. Periodic solutions were obtained, as is seen in Figs 1-2 and 1-3 but they do have a phase lag. It should therefore be possible to superpose a diagram of a flow field with a random cycle diagram of another flow field differing by 0.5 cycle from the first. This has been proved (Fig 1-2). As will be seen from a diagram (Fig 1-4) of quasi-steady pressure distribution and diagrams (Figs 1-5 and 1-6) of unsteady pressure distribution, the absolute value of unsteady pressure distribution coefficient is greater on the forward part of the airfoil. This is the part on which generation, growth and decay of shock waves take place.

(Case 2) Numerical capturing of unsteady phenomena in displacement of a strong shock wave

Under the condition of a free stream Mach number of 0.72, a strong and persistent shock wave is produced on the upper surface of a Joukowski airfoil at an angle of attack of 0° , 2° or 4° . Unsteady calculations with $k = 0.1$ and 0.25 were made under conditions of a mean angle of attack 2° and an amplitude of oscillation of 2° . With either value of k , the maximum amplitude of displacement (Fig 2-5b&c) of C_p in a period was smaller than an absolute difference (Fig 2-5a) in C_p between two steady flows having angles of attack equal to 0° minimum and 4° maximum. It will be seen from Figs 2-3 and 2-4 that the supersonic region continues to enlarge even after passing the time (planes C in these figures) of a maximum angle 4° of attack, and continues to shrink after passing the time (planes G in the figures) of minimum 0° angle of attack, indicating a phase lag. In the unsteady pressure distribution, Fig 2-7 shows a pressure peak originating from the displacing shock wave. With an increase in frequency parameter k , the pressure peak deviates gradually from the real part to the imaginary part. In other words, with an increase in frequency, periodic shock wave motion increases the time lag. It will be seen from Fig 2-8, which illustrates unsteady pressure distribution with absolute values and phase angle, the width and height of a pressure peak, which is coupled to shock wave, decreases with an increase in frequency. This was caused by a reduction in amplitude of displacement with an increase in frequency.

Coefficients up to the third harmonic of tangential force (C_X), normal force (C_Y), pitching moment (C_M) (about centre of half chord and positive nose-up), and the position of shock wave (S_X) (position of lowest pressure on the upper surface), which were given by Fourier analysis in section (6c) of the previous section, are shown in Table 3. At either value of k , the ratio of the second harmonic to the first harmonic in the coefficient of normal force or coefficient of tangential force is smaller than 0.06. It is therefore indicated that the loci of these coefficients are close to sine curves incorporating different types of time lag, despite the presence of an oscillating shock wave. However for the coefficient of tangential force and the position of shock wave, the ratios are greater than 0.1. In other words, it is clear that these two coefficients deviate from sinusoidal loci and behave nonlinearly. With an increase in the value of k from 0.1 to 0.25, considerable reduction in absolute values of the first harmonics and increases in their phase angles, except that of C_Y , were observed.

Table 3

Fourier coefficients for coefficient of chord force (C_X), coefficient of normal force (C_Y), coefficient of pitching moment (C_M) (about centre of half-chord, positive nose-up) and the position of shock wave (S_X)

(a) $k = 0.1$

f	Mean	Amplitudes			Phase angles		
	B_0	A_1	A_2	A_3	ϕ_1	ϕ_2	ϕ_3
C_X	0.0047	0.0064	0.0034	0.0004	-32.97	48.77	116.79
C_Y	1.0685	0.2176	0.0052	0.0012	-18.34	17.68	-156.84
C_M	0.0813	0.0292	0.0016	0.0004	-22.02	0.44	40.71
S_X	0.6058	0.0340	0.0040	0.0002	-36.31	21.94	175.13

(b) $k = 0.25$

f	Mean	Amplitudes			Phase angles		
	B_0	A_1	A_2	A_3	ϕ_1	ϕ_2	ϕ_3
C_X	0.0024	0.0040	0.0026	0.0004	-66.79	29.33	94.10
C_Y	1.0505	0.1586	0.0014	0.0006	-15.96	-34.68	-145.20
C_M	0.0858	0.0270	0.0002	0.0000	-27.61	33.16	59.90
S_X	0.5968	0.0240	0.0032	0.0006	-70.79	-60.27	-149.50

(Case 3) Capturing of an unsteady flow containing strong diagonal shock wave always present at the trailing edge on the upper surface (downstream is subsonic), and shock wave periodically displacing downstream of the trailing edge on the lower surface

At a main stream Mach number of 0.92, a steady shock wave is present at the trailing edge on the upper surface of a Joukowski airfoil where the angle of attack is -3° , 0° or 3° , as shown in Figs 3-2 and 3-4a. On the lower surface, the position of another shock wave moves a large distance upstream from the trailing edge with an increase in angle of attack. Where the mean angle of attack is 0° , the amplitude of pitching is 3° and the frequency is 0.1, the unsteady shock wave (Fig 3-3) on the lower surface moves periodically within a range surrounded by two steady shock waves (Fig 3-2) produced at an angle of attack $\pm 3^\circ$. It will be seen from Fig 3-4 that the variation of C_p within the period relevant to $k = 0.1$ is smaller than that of C_p of a quasi-steady flow. As will be seen from Figs 3-5, 3-6 and 3-7, the pressure coefficient for unsteady flow is a flat curve close to 0 on the upper surface because of an almost fixed shock wave, but the absolute values vary widely on the rear half-chord because of the large movement of the shock wave.

(Case 4) Capturing numerical values of 'fish tail' shock wave system and the process of its degradation

The appearance of the so-called 'fish tail' shock wave system is well known when the free stream Mach number is close to 1. That is, weak oblique shock waves (flow changing from supersonic to supersonic) attach to the trailing edge on the upper and lower surfaces and merge with a normal shock wave downstream of the trailing edge. In this triangular region formed by these three shock waves, there is no great variation in Mach number. At a free stream Mach number of 0.93, a shock wave system having a similar structure was obtained with a Joukowski airfoil when the angle of attack was -3° . However, when the angle of attack was 0° , a fairly small subsonic region appeared behind a steady shock wave in the vicinity of the trailing edge on the lower surface. When the angle of attack was 3° , this subsonic region was much bigger. (Fig 4-1, a slip flow was present at a position where a sonic line of a normal shock wave changed rapidly downstream of the trailing edge). An unsteady solution was then sought under conditions of mean angle of attack 0° , amplitude of pitching 3° and frequency parameter 0.1. During the process of obtaining the periodic solution shown in Fig 4-2, a 'fish tail' shock wave system was maintained at time points G, H and A (angles of attack, $-3^\circ \rightarrow -1.5^\circ \rightarrow 0^\circ$), a supersonic region spread out in the vicinity of the trailing edge on the lower surface with an advance in time points to B, C and D ($1.5^\circ \rightarrow 3^\circ \rightarrow 1.5^\circ$), it contracted with an advance to D, E and F ($1.5^\circ \rightarrow 0^\circ \rightarrow -1.5^\circ$), and disappeared at time point G (-3°). As compared with the previous case (Fig 3-3), the shock wave on the upper surface (Fig 4-2) leaned considerably towards the direction of the chord line. The diagrams (Figs 4-3, 4-4, 4-5 and 4-6) of steady and unsteady pressure distribution on the airfoil surface differed considerably from the previous case in the patterns of flow in the vicinity of and downstream of the trailing edge, but were the same in trend. However, the peak in an absolute value of unsteady pressure coefficient caused by the shock wave on the lower surface was smaller.

(Case 5) Capturing numerical values of an unsteady flow about an airfoil where the main stream Mach number is greater than 1

When the free stream Mach number exceeds 1 an isolated shock wave forms upstream of a circular leading edge, which is almost normal to the air flow in the vicinity of the chord line, thus it becomes subsonic downstream of it. However, it is well known that this is accelerated again to supersonic speed on the airfoil surface, and a weak oblique shock wave (its flow changing from supersonic to supersonic) forms at the trailing edge. Here again, in respect of a Joukowski airfoil, similar steady flow patterns were obtained under conditions of a free stream Mach number of 1.4 and angles of attack of -5° , 0° and 5° (Figs 5-1 and 5-3a). The supersonic region in the vicinity of the leading edge was the greatest where the angle of attack was -5° . In other words, an isolated shock wave was the smallest. According to the results (Figs 5-2 and 5-3b) of calculating an unsteady flow under conditions of a mean angle of attack 0° , amplitude of pitching 5° and frequency parameter of 0.1, it was something which could be visualised from a steady flow pattern at a mean angle of attack 0° . The quasi-steady pressure distribution (Fig 5-4) and unsteady pressure distributions (Figs 5-5 and 5-6) were lower in absolute values than in any of the above cases, and they formed flat curves and the phase lag was small.

5.2 Comparisons of the results of the present method with experiments and other methods of calculation

(Case 6) A flow field having an extensive supersonic field, terminated by a relatively strong shock wave

This flow field, which was of the same type as that used in case 2, was used in the calculations for the NLR 7301 airfoil* in order to facilitate comparison with the experiments ($M_\infty = 0.7$) of Tijdeman¹. Tijdeman carried out experiments with steady flows in relation to amplitudes $\alpha = 2.5^\circ$, 3.0° and 3.5° of pitching, and obtained the pressure distributions shown in Figs 6-4a and 6-5a. He then carried out experiments with unsteady flow about an airfoil subjected to oscillation in pitch, $\alpha(t) = 3^\circ + 0.5^\circ \sin 0.384t$, around a central axis ($X_c = 0.4$, $Y_c = -1/60$). The method of calculation we used was for inviscid flow, but the experimental results will have the influence of viscosity and the effect of the wind tunnel. Accordingly, steady flow calculations were made for $M_\infty = 0.7$ and varying angles of attack, the angle of attack $\alpha = 1.5^\circ$ (Figs 6-4b, 6-5b and 6-2), was chosen as having pressure distribution closest to the results of experiments carried out at $\alpha = 3.0^\circ$. The value 1.5° was used as a mean angle of attack in the calculations of the unsteady flow (Fig 6-3). The amplitude of displacement of C_p during one period of this unsteady flow was smaller than that in the quasi-steady flow, as will be seen from Fig 6-4. Quasi-steady pressure distribution and the unstable pressure distribution, have a high pressure peak (Figs 6-5, 6-6, 6-7 and 6-8) caused by shock wave, as in case 2. This is common to the calculated results and the experiments. However this peak cannot be predicted from the solution based on thin airfoil theory**, also shown in these figures. The results of calculations made by the present method are in good qualitative agreement with experimental results, except for a slight deviation in the position of the shock wave and differences in absolute values of steady and unsteady pressure coefficients.

(Case 7) Unsteady phenomena of an airfoil under design conditions of being shock wave-free

The supercritical shock-free airfoil NLR 7301 for $M_\infty = 0.721$ and $C_L = 0.595$ has been designed using hodograph theory. In the experiments made by Tijdeman, in which the effects of viscosity and tunnel walls were included, values $M_\infty = 0.744$ and $\alpha = 0.85^\circ$ were found to give a C_p curve approximating the C_p curve under design conditions. In the experiment, an increase in angle of attack by 0.5° produced a shock wave on the upper surface, and a decrease by 0.5° produced no shock wave but two peaks in the C_p curve. As will be seen from the above, a slight change in angle of attack produced a great change in steady pressure distribution on the upper surface but only a small change

* This airfoil had been designed by the hodograph method²¹ of Boerstoeel for obtaining a flow free of shock waves. Being relatively thick (maximum thickness 16.5%) and blunt-nosed, this is considered to be representative of modern supercritical airfoil designs. Because of its shape, the hypothesis of small disturbance is liable to be violated and a small disturbance equation cannot be used. The full potential equation or the Euler equations should be used. The Cartesian grid system proposed by Carlson and used by Isogai⁷ is unsuitable for this type of airfoil with a blunt nose.

** It has been shown by experiments that an equation approximating a thin airfoil can be used satisfactorily for making predictions relating to subsonic and supersonic flows, but it is known¹ that the equation does not closely agree with experimental results in the case of supercritical flow.

on the lower surface (Fig 7-4a). In these calculations, values of $M_\infty = 0.721$ and $\alpha = -0.19^\circ$ were found to give an approximation to the C_p curve under the design conditions. This resultant angle of attack $\alpha = -0.19^\circ$ was used as the standard from which steady pressure distributions were obtained when the angle of attack was increased or decreased by 0.5° (Fig 7-4b). As is seen from the isobaric contours shown in Fig 7-2, a small change in the angle of attack results in a large change in the flow field from the design conditions. The quasi-steady pressure distribution (Fig 7-5), has a broad bulge on the upper surface in both experimental results and the results of the present calculation. The curve from thin airfoil theory differs qualitatively from these, indicating that thin airfoil theory is unsuitable for prediction.

Unsteady phenomena resulting from the choice of $\Delta\alpha = 0.5^\circ$ and $k = 0.181$ and the design conditions are as follows. The unsteady pressure distribution (Fig 7-3) on the lower surface became a relatively smooth curve and there was good agreement between the experimental results and the results of the present calculation. On the upper surface, the shape was similar but there was a quantitative difference. Referring to Fig 7-7, curves for absolute values of the unsteady pressure distribution coefficient obtained in the experiment and the present calculation have a peak resulting from periodic formation (Fig 7-3) of a weak shock wave and the phase curves are smooth for about 40~50% of the chord length and then they turn upwards sharply owing to the presence of the shock wave. As in the case of quasi-steady flow, the results of thin airfoil theory differed considerably from those of the experiment and the present calculation. As is seen from the above, the results of using our method based on the inviscid theory differ quantitatively from those of experiment, but qualitatively they capture principal characteristics of an unsteady flow about an oscillation about the shock-free design condition.

Remark: The wind tunnel used by Tijdeman in his experiment was capable of producing a relatively low Reynolds number of only 2.2×10^6 . This signifies that the transition from laminar flow to turbulent flow in that wind tunnel takes place downstream of that in free flight ($Re = 30 \sim 50 \times 10^6$). Tijdeman also carried out an experiment with a transition zone fixed at 30% chord, which is similar to that in free flight. Under the condition of a strong shock wave in case 6, there was no effect of a transition zone because spontaneous transition occurred at about the same position, but it will be seen from Figs 7-8 and 7-9 that a flow was very sensitive to the transition zone under the design condition in that case. It will also be seen from the figures that the results of the present calculations, which did not include the effects of viscosity or turbulent flow, were closer to the results of experiments with a transition zone than to those of experiments in spontaneous transition without a transition zone. It is difficult to say that the flow field in this experiment, undesirable phenomena of the formation of an oblique compression wave from the transition zone, and its transformation into a compression wave on being reflected by a sonic line were observed. All the same, a flow under the design conditions reacts very sensitively to a slight change in condition.

(Case 8) Unsteady transonic wave accompanied by a weak shock wave

Davis, et al.² carried out experiments with the symmetrical airfoil NACA 64A010, with a fine and rounded leading edge, with free stream Mach number 0.8. Numerical solutions for it were sought by Magnus^{2,22}, using the Euler equations, on assuming inviscid flow, and by Isogai⁵ who used a full potential equation and a transonic small disturbance (TSD) equation. Similarly, we sought three steady flows under the conditions of the same free stream Mach number and angle of attack of 0° to 1° . Also we obtained unsteady flows at the mean angle of attack 0° and in amplitude of pitching 1° , for comparison. Isobaric contours and C_p curves for steady and unsteady flows obtained by the present method of calculation are shown in Figs 8-2, 8-3 and 8-4. The airfoil being symmetrical and having a mean angle of attack of 0° , the flow field at a certain cycle in Fig 8-3 is the same as the inversion of a flow field at a cycle differing by 0.5 in absolute value. The steady flow shown in Fig 8-2 (Fig 8-4) has no supersonic region (shock wave absent) on the lower surface when the angle of attack is 1° , but the unsteady flow shown in Fig 8-2 (Fig 8-4) has supersonic regions (a shock wave present) on both upper and lower surfaces at all cycles. Comparisons of the results of the experiment, the present calculation, and other calculations are shown in Figs 8-5 to 8-8. In the steady pressure distribution (Fig 8-5) at angle of attack 0° , the shock wave according to the present calculation is located upstream of the others, but its width is the smallest, followed by a fall. The present method of calculation captured the shock wave sharply. The peak resulting from the periodic displacement of the shock wave in the unsteady pressure distribution were obtained in decreasing order of size (Figs 8-7 and 8-8) from Magnus' method using the Euler equations, the present method using the same equations, Isogai's method using a full potential equation, and Isogai's method using a small disturbance potential equation. Considering the characteristics of these equations, this order seems appropriate. Obtaining different results (Fig -6) from using the same Euler equations resulted from differences in grid system and the finite difference method. Among the methods used, those which were particularly close to unsteady experimental values were the present method and Isogai's method using the full potential equation. The results from both methods approached the experimental values, thus they both seem to be satisfactory for prediction in this case. This case, in which the airfoil thickness is small and the leading edge is sharp, is also particularly suitable for Isogai's method using the small disturbance potential equation in which the airfoil slope is handled on a flat plate or the method of Isogai using a full potential equation employing a Cartesian grid system which is considered to be weak when used for thick and rounded leading edges.

Remark: Because of the use of a maximum number of grid points of 121×31 in the program, no satisfactory solution could be expected in this case. Accordingly, a $\Delta x/4$ -wide grid prepared for use only in the vicinity of vertically asymmetrical shock wave was used vertically symmetrically in the vicinity of the leading edge.

5.3 Required computing time

The computing times required for the calculation of numerical values in sections 5.1 and 5.2, using a FACOM 230-75 computer [CPU (ordinary computer) + APU (array processor)], in accordance with the routine described in section 4 are as follows:

- | | |
|--|------------------------------|
| (1) the formation of a single grid and the computation of associated differential coefficients | about 25 seconds with CPU |
| (2), (3) computation of one steady flow | about 20~90 seconds with APU |
| (4) the processing of results pertaining to a quasi-steady flow | about 9 seconds with CPU |
| (5) computation of an unsteady flow cycle | about 25~30 seconds with APU |
| (6) processing of results pertaining to an unsteady flow | about 20 seconds with CPU. |

Most of the computing times were used in performing routines (2) and (3), using program FLOW. In the computation of steady flows under (2) and (3), the time requirement varied greatly according to the division of time chosen for the selection of initial values and for maintaining the complexity and stability of flow patterns. The processing of results pertaining to an unsteady flow in (5) is similar, but it depends on frequency parameter and is independent of the selection of initial values. The average total time required in the case of computing for quasi-steady flow and four cycles of unsteady flow was about 5 hours.

5.4 Deviation from Rankine-Hugoniot relation

The following Rankine-Hugoniot relation holds theoretically in a steady normal shock wave in an inviscid flow

$$\frac{P_2}{P_1} = 1 + \frac{\gamma}{\gamma + 1} (M_1^2 - 1) .$$

In the above equation, the subscripts 1 and 2 indicate positions immediately before and after the shock wave. The suitability of a particular numerical solution as a solution for an inviscid flow can be judged by the degree of its closeness to the Rankine-Hugoniot relation.

With a view to finding the suitability of the present method of calculation, the quasi-steady and steady flows (13 in number) which could be considered to contain normal shock waves were selected from among those obtained in the examples of numerical calculations referred to earlier. Pressure rise at a shock wave was obtained from Mach number and pressure obtained at the actual mesh points. These values are plotted together with results of other methods of calculation in a diagram (Fig 9) devised by Lomax, et al.²³. As expected, the solutions by time-dependent methods based on the Euler equations, including the solution by the present method of calculation were found to better satisfy the Rankine-Hugoniot relation than solution by a relaxation method based on a potential equation.

However, because of the presence of a boundary layer in the experiment, the strength of the shock wave measured on an airfoil is generally lower than what can be predicted from the above relation. Because of this, a numerical solution using a potential equation which is lower in degree of approximation than Euler equations for an inviscid flow can often be closer to an experimental result. For obtaining a solution justifiably closer to an experimental value, it is necessary to solve Navier-Stokes' equation for viscous flow.

6 CONCLUSION

This work proposes a method for the calculation of an inviscid compressible flow about a two-dimensional airfoil oscillating sinusoidally in pitch. With a view to handling accurately an airfoil even with a rounded and thick leading edge (such as the NLR 7301 airfoil), which appears difficult to solve by previously-published methods for calculating unsteady flows. A coordinate transformation was devised and a computational plane formed. The Euler equations which have no approximation were used to model an inviscid flow, and the finite difference method of Lax-Wendroff with artificial viscosity was used for its solution. Then, the effectiveness of the present method was examined by carrying out numerical calculations, using four airfoils (Joukowski, NACA 0012, NLR 7301 and NACA 64A010 airfoils) within a wide range ($0.7 \sim 1.4$) of Mach number. Consequently, we succeeded in numerically capturing various types of unsteady shock wave phenomena (processes of generation, growth and disappearance of a weak shock wave, processes of propagation of a strong shock wave, a 'fish tail' shock wave system and its process of decaying, the process of propagation of a shock wave separated from the leading edge, and others). During this time, we proved, as was expected, that the discontinuities across captured shock waves satisfy better the Rankine-Hugoniot relations than do those calculated using the fuel potential equation. The present method of calculation seems fully workable for predicting inviscid and unsteady aerodynamic phenomena but is unsuitable for unsteady flow with a strong viscous interference. If a more powerful computer than is now available became available in the near future then it should be possible to get numerical solutions for unsteady flows with strong viscous interference by modelling the viscous flow.

The author is grateful to Technical Officer Isogai for participating in the discussion and for supplying the data.

REFERENCES

- | <u>No.</u> | <u>Author</u> | <u>Title, etc</u> |
|------------|--|---|
| 1 | H. Tijdeman | Investigations of the transonic flow around oscillating airfoils.
NLR TR 77090U, National Aerospace Laboratory, Netherlands (1977) |
| 2 | S.S. Davis
C.N. Malcolm | Experiments in unsteady transonic flows.
AIAA Paper 79-0769 (1979) |
| 3 | W.F. Ballhaus
P.M. Goorjian | Implicit finite difference computations of unsteady transonic flows about airfoils, including the treatment of irregular shock wave motions.
AIAA Paper 77-205 (1977) |
| 4 | N.J. Yu
A.R. Seebass
W.F. Ballhaus | An implicit shock-fitting scheme for unsteady transonic flow calculations.
AIAA Paper 77-633 (1977) |
| 5 | K. Isogai | Numerical calculations of unsteady air force at transonic speed. Preprint, fiscal year 1979, Tech Meeting National Aerospace Laboratory, pp.7-8 |
| 6 | K. Isogai | Numerical study of transonic flow over oscillating airfoils using the full potential equation.
NASA Technical Paper 1120 (1978) |
| 7 | K. Isogai | Calculation of unsteady transonic flow over oscillating airfoils using the full potential equation.
AIAA Paper 77-448 (1977) |
| 8 | R. Chipman
A. Jameson | Fully conservative numerical solutions for unsteady irrotational transonic flow about airfoils.
AIAA Paper 79-1555 (1979) |
| 9 | R.M. Beam
R.F. Warming | An implicit finite difference algorithm for hyperbolic systems in conservation-law form.
J. Comput. Phys., Vol.22, pp.87-110 (1976) |
| 10 | R. Magnus
H. Yoshihara | Finite difference calculations of the NACA 64A410 airfoil oscillating sinusoidally in pitch at $M_\infty = 0.72$.
Technical Report CASD-NSC-74-004, Convair Division of General Dynamics (1974) |
| 11 | R.J. Magnus
H. Yoshihara | Calculations of transonic flow over an oscillating airfoil.
AIAA Paper 75-98 (1975) |
| 12 | R. Magnus
H. Yoshihara | Unsteady transonic flows over an airfoil.
AIAA Journal, Vol.13, No.12, pp.1622-1628 (1975) |
| 13 | R. Magnus
H. Yoshihara | The transonic oscillating flap.
AIAA Paper 76-327 (1976) |

REFERENCES (concluded)

- | <u>No.</u> | <u>Author</u> | <u>Title, etc</u> |
|------------|--|--|
| 14 | R.J. Magnus | Computational research on inviscid, unsteady, transonic flow over airfoils.
CASD LVP 77-010, Convair Division of General Dynamics (1977) |
| 15 | A. Lerat
J. Sides | Numerical calculation of unsteady transonic flows.
ONERA TP 1977-19E (1977) |
| 16 | A. Lerat
J. Sides | Numerical simulation of unsteady transonic flows using the Euler equations in integral form.
ONERA TP 1979-10 (1979) |
| 17 | W.J. Chyu
S.S. Davis | Calculation of unsteady transonic flow over an arbitrary airfoil.
AIAA Paper 79-1554 (1979) |
| 18 | T. Ishiguro | Numerical calculations of inviscid compressible flow about two-dimensional airfoils.
Technical Report National Aerospace Laboratory, TR-489 (1977) |
| 19 | T. Ishiguro | Numerical calculations of inviscid compressible flows about two-dimensional airfoils.
J. Japan Soc., Aeronautics and Space, Vol.25, No.278, pp.118-124 (1977) |
| 20 | T. Ishiguro | Finite difference calculations of transonic flows over oscillating airfoils.
Theoretical & Applied Mechanics, Vol.28, pp.421-432 (1980) |
| 21 | J.W. Boerstoeel | Design and analysis of a hodograph method for the calculation of supercritical shock-free airfoils.
NLR TR 77046U (1977) |
| 22 | M.H. Williams | Unsteady airloads in supercritical transonic flows.
AIAA Paper 79-0769 (1979) |
| 23 | H. Lomax
F.R. Bailey
W.F. Ballhaus | On the numerical simulation of three-dimensional transonic flow with application to the C-141 wing.
NASA TND-6933, p.28 (1973) |



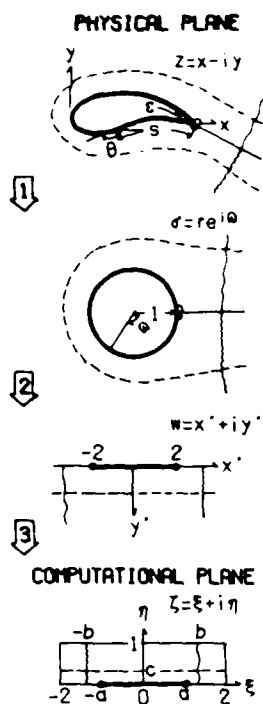


Fig I Mapping from the physical plane on to the computational plane

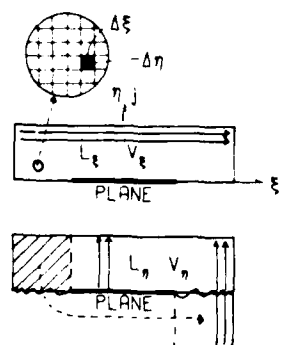


Fig II Direction of operator

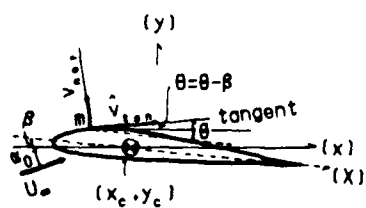


Fig III Description of sinusoidal pitching

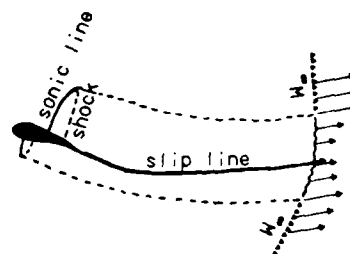


Fig IV Handling of downstream at infinity

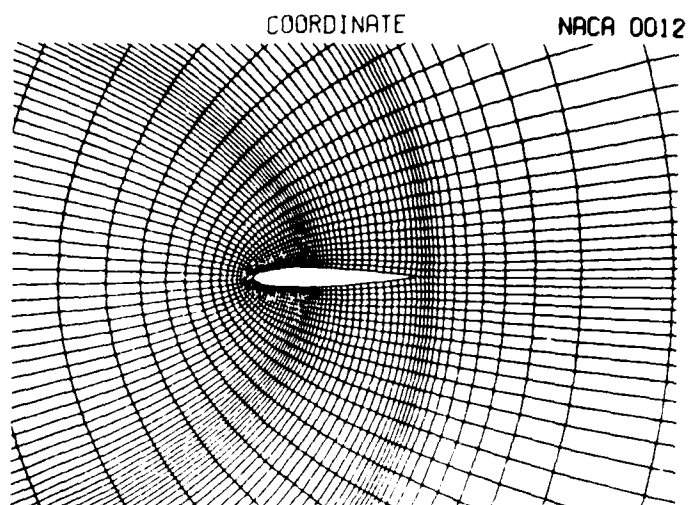


Fig 1-1 Grid image on the physical plane

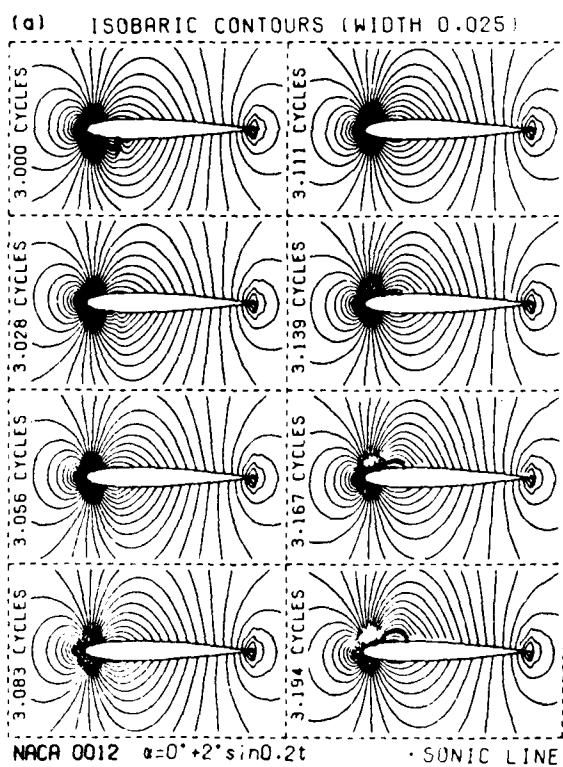


Fig 1-2a Unsteady isobaric contour

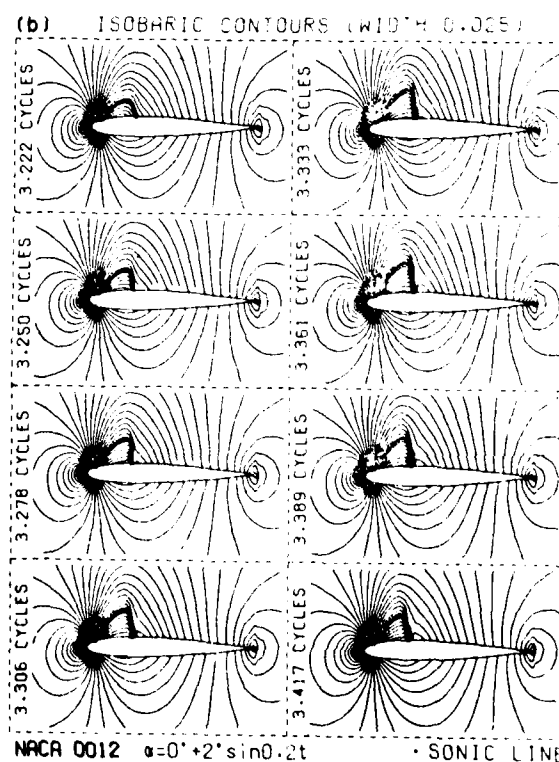


Fig 1-2b Unsteady isobaric contour

Figs 1-2c - 1-2f

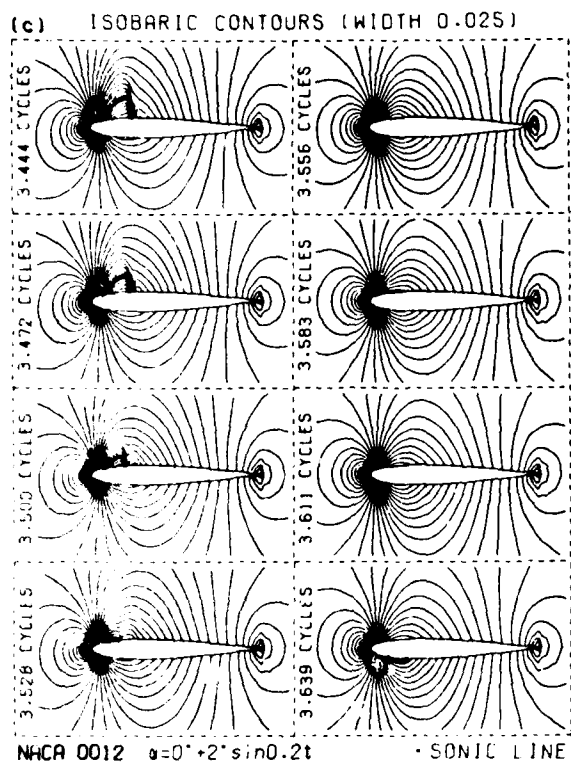


Fig 1-2c Unsteady isobaric contour

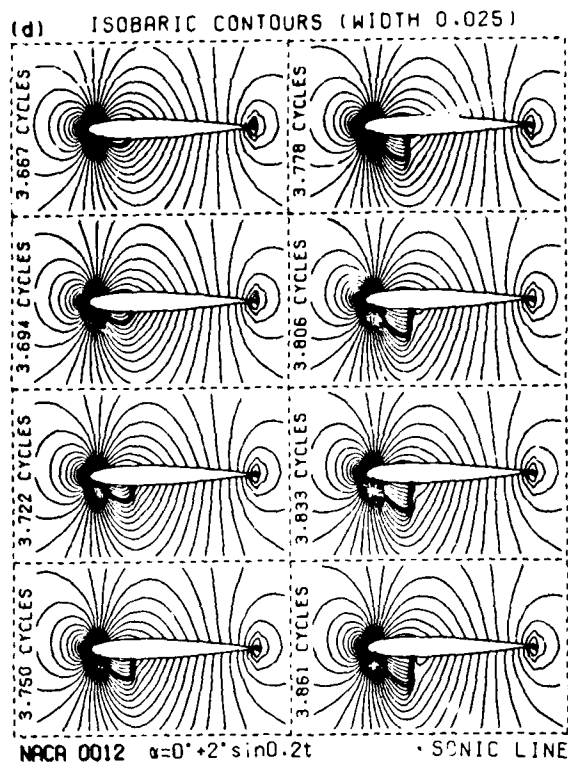


Fig 1-2d Unsteady isobaric contour

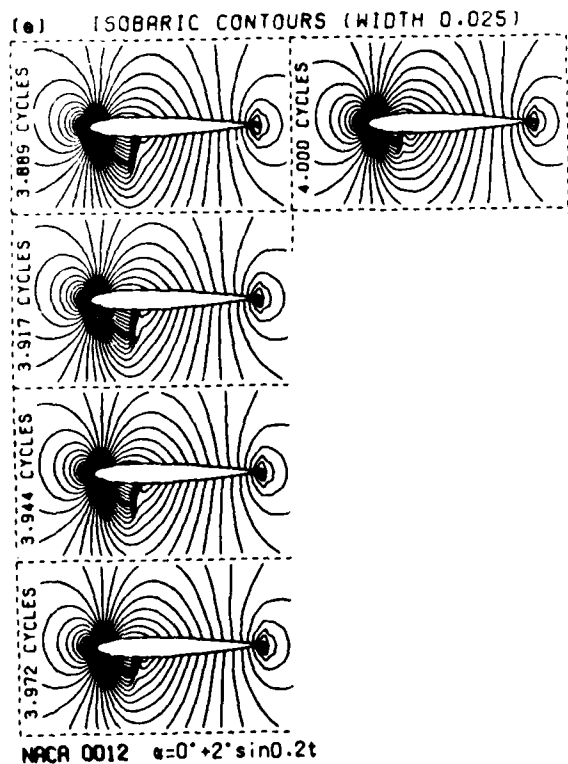


Fig 1-2e Unsteady isobaric contour

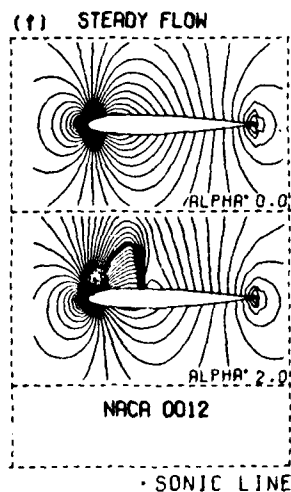


Fig 1-2f Steady isobaric contour

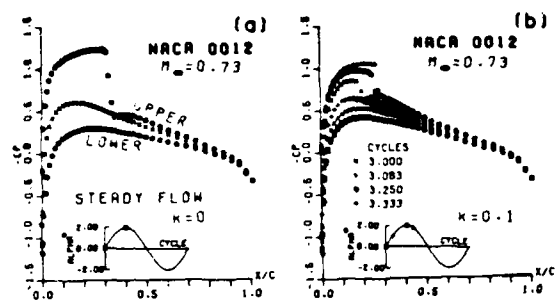


Fig 1-3 Steady and unsteady pressure coefficients

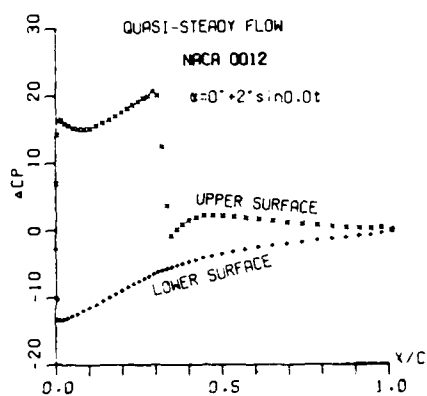


Fig 1-4 Quasi-steady pressure distribution

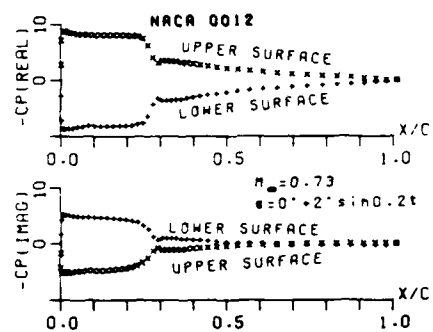


Fig 1-5 Unsteady pressure distributions

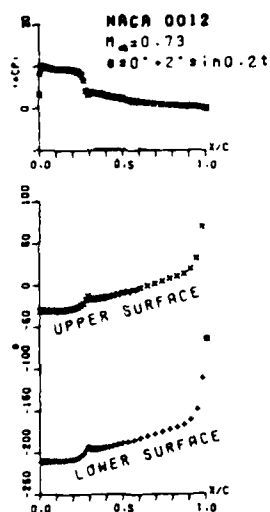


Fig 1-6 Unsteady pressure distributions

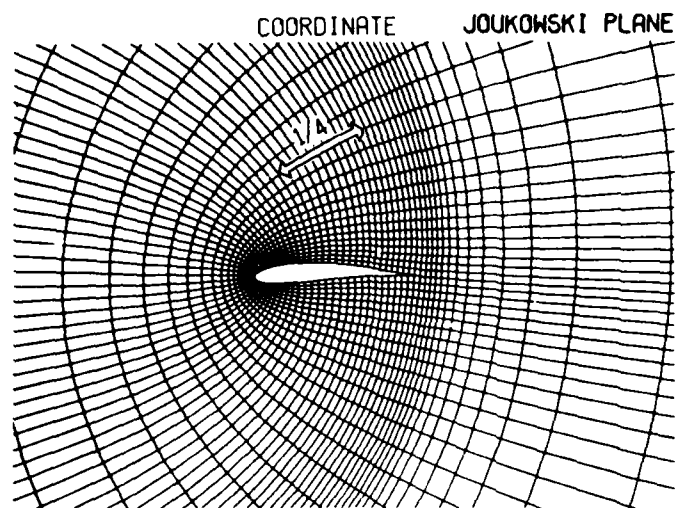


Fig 2-1 Grid image on the physical plane

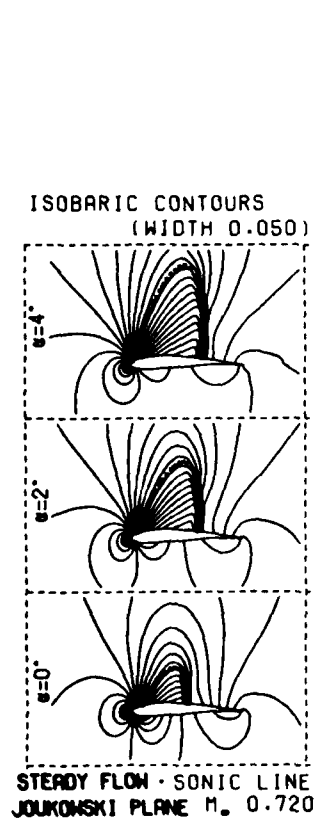


Fig 2-2 Steady isobaric contours

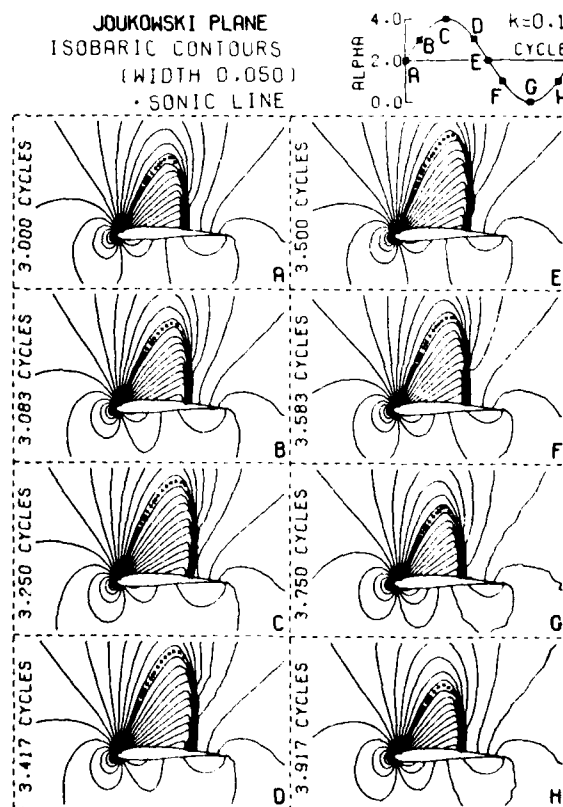


Fig 2-3 Unsteady isobaric contours $k = 0.1$

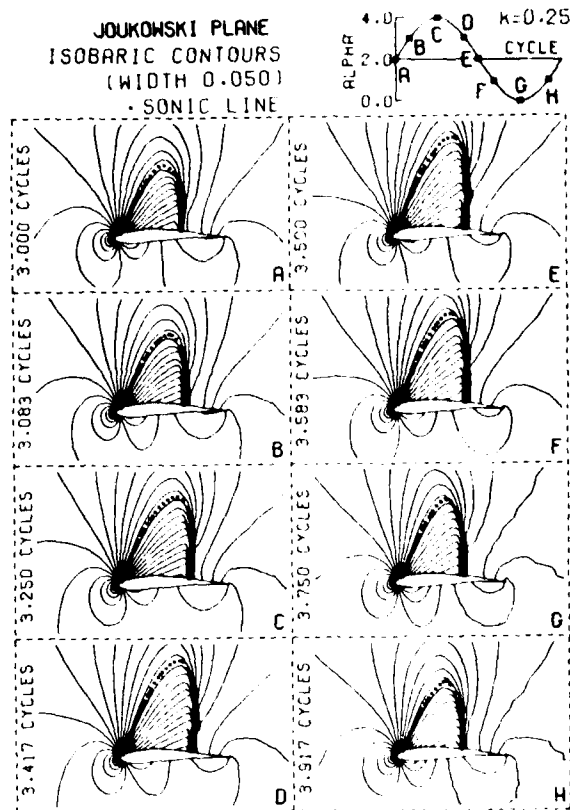


Fig 2-4 Unsteady isobaric contours $k = 0.25$

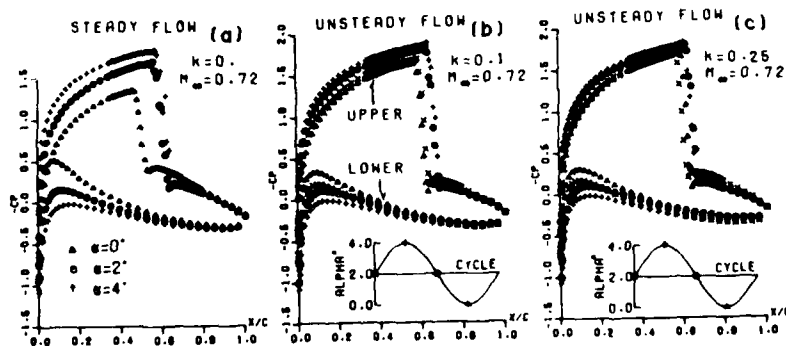


Fig 2-5 Steady and unsteady pressure coefficients

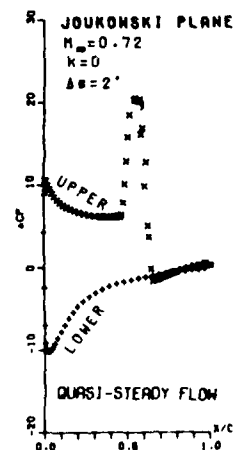


Fig 2-6 Quasi-steady pressure distribution

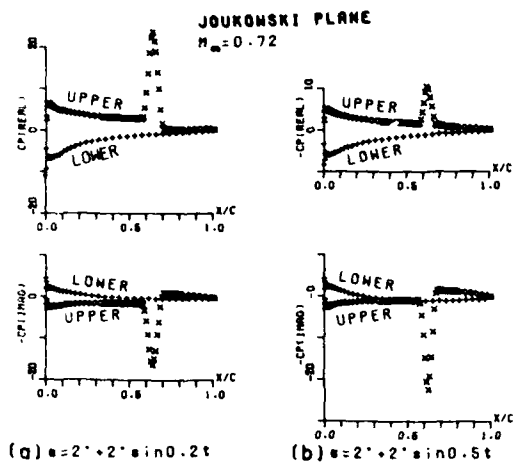


Fig 2-7 Unsteady pressure distributions

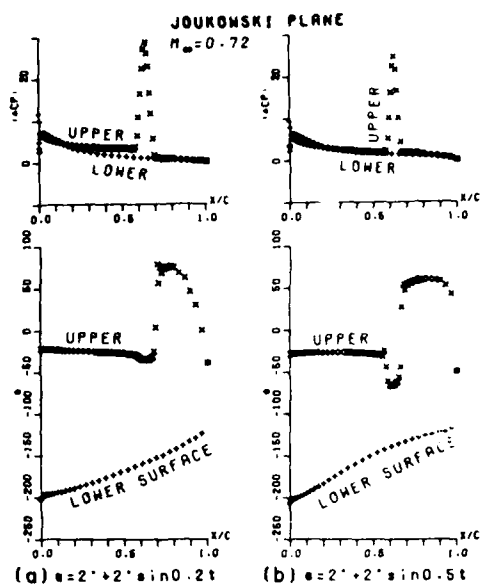


Fig 2-8 Unsteady pressure distributions

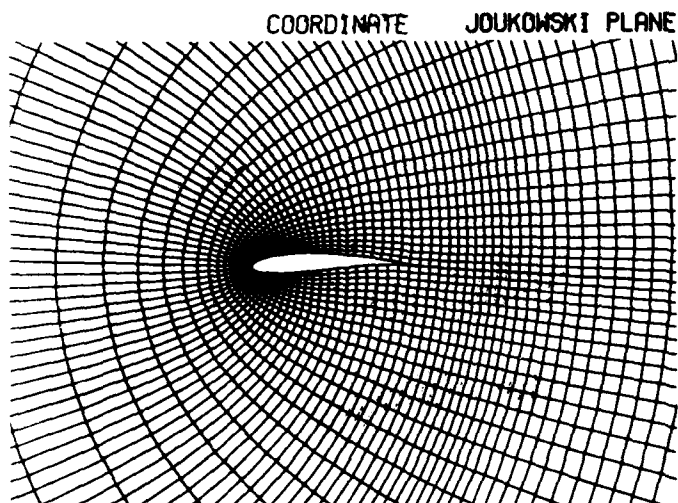


Fig 3-1 Grid image on the physical plane

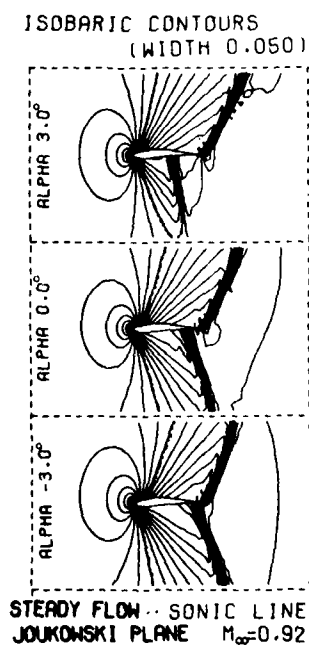


Fig 3-2 Steady isobaric contours

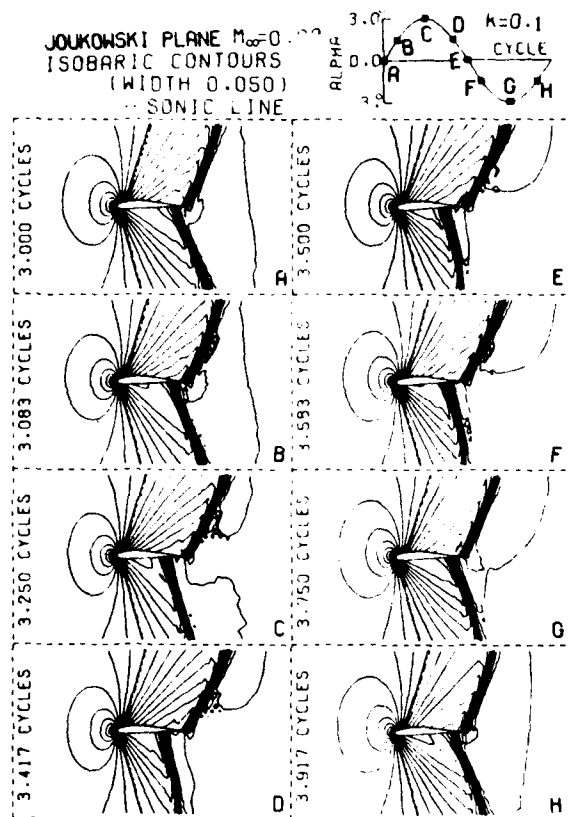


Fig 3-3 Unsteady isobaric contours

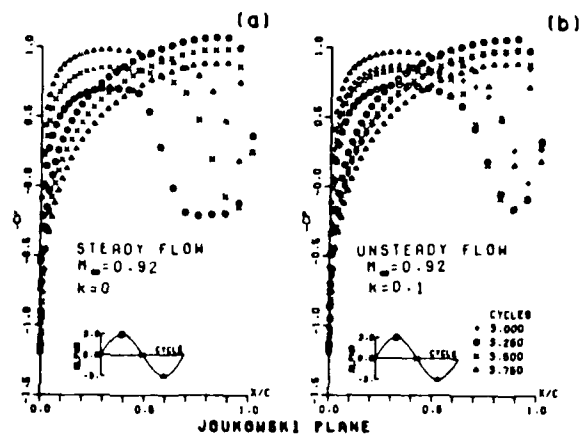


Fig 3-4 Steady and unsteady pressure coefficients

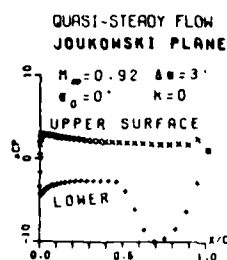


Fig 3-5 Quasi-steady pressure distribution

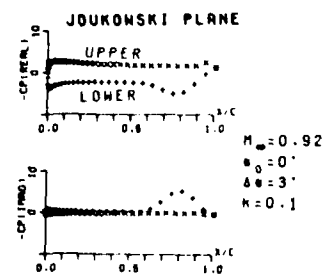


Fig 3-6 Unsteady pressure distributions

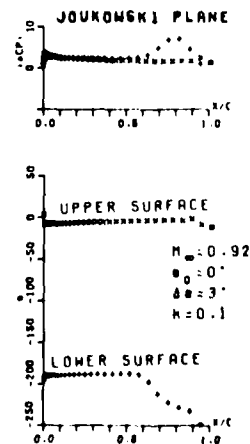


Fig 3-7 Unsteady pressure distributions

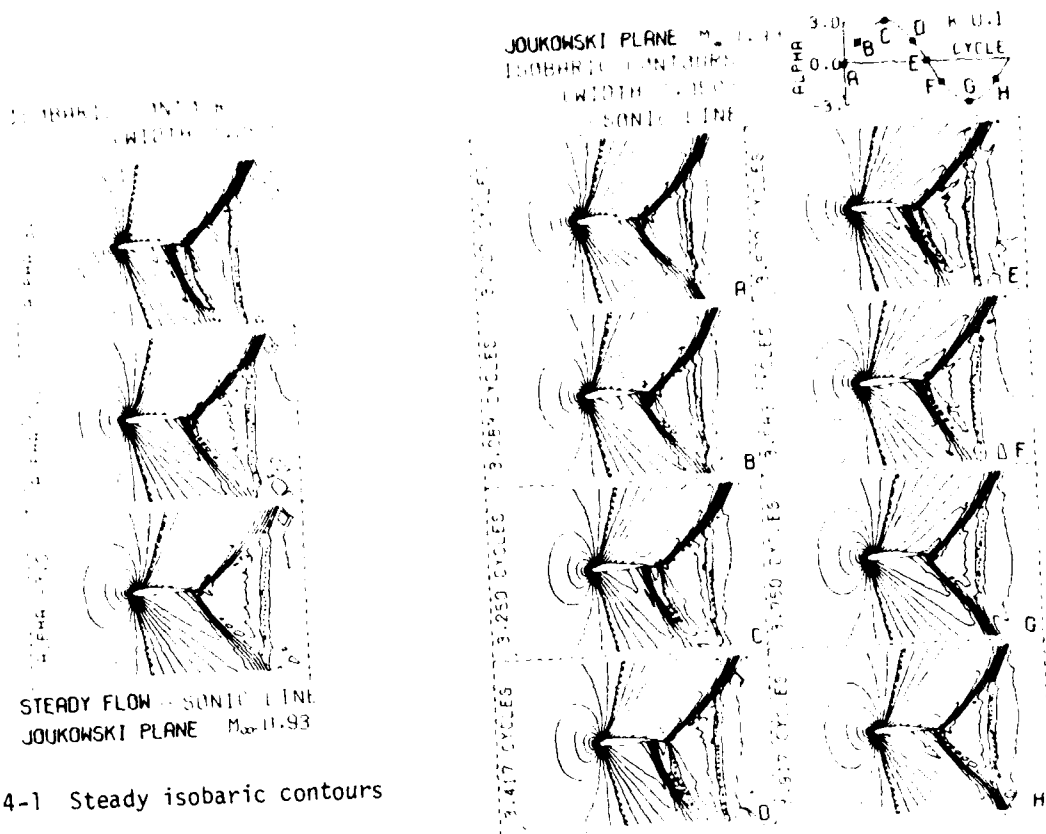


Fig 4-1 Steady isobaric contours

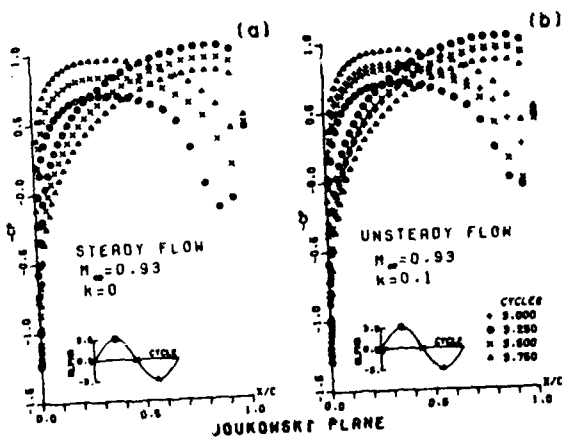


Fig 4-3 Steady and unsteady pressure coefficients

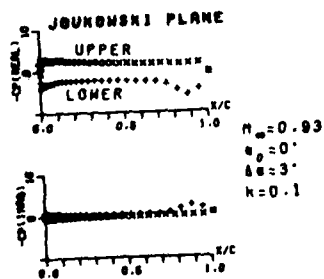


Fig 4-5 Unsteady pressure distributions

Fig 4-2 Unsteady isobaric contours

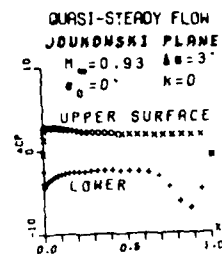


Fig 4-4 Quasi-steady pressure distribution

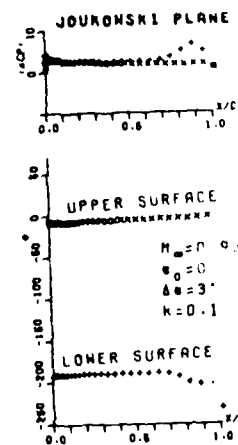
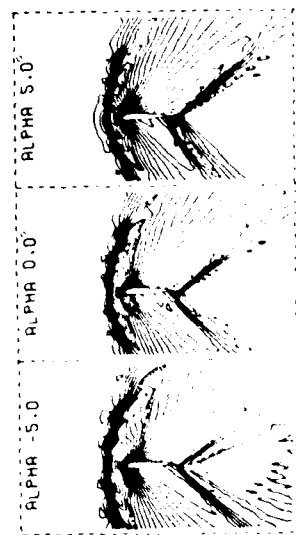


Fig 4-6 Unsteady pressure distributions

ISOBARIC CONTOURS
(WIDTH 0.025)



STEADY FLOW - SONIC LINE
JOUKOWSKI PLANE $M_\infty=1.4$

Fig 5-1 Steady isobaric contours

JOUKOWSKI PLANE $M_\infty=1.4$
ISOBARIC CONTOURS
(WIDTH 0.025)
SONIC LINE

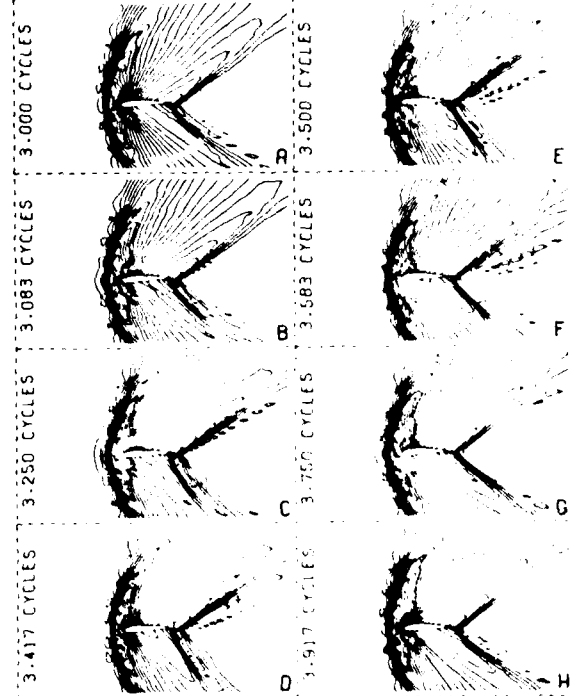


Fig 5-2 Unsteady isobaric contours

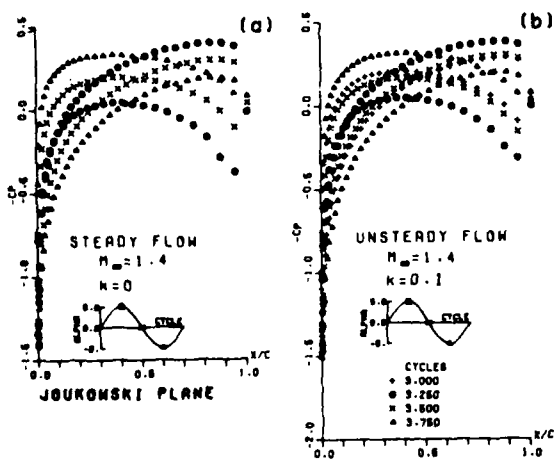


Fig 5-3 Steady and unsteady pressure coefficients

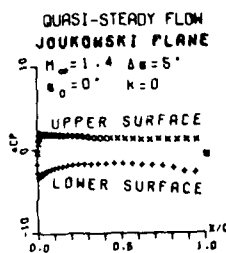


Fig 5-4 Quasi-steady pressure distribution

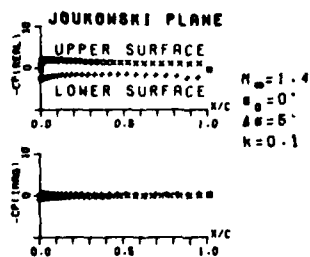


Fig 5-5 Unsteady pressure distribution

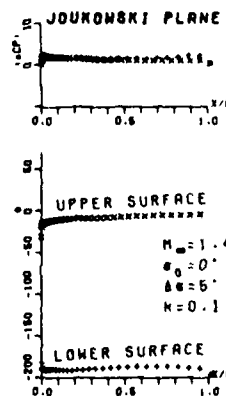


Fig 5-6 Unsteady pressure distribution

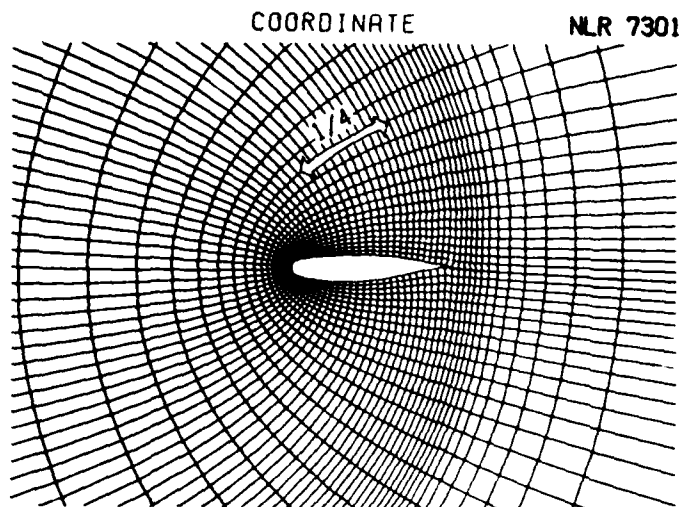


Fig 6-1 Grid image on the physical plane

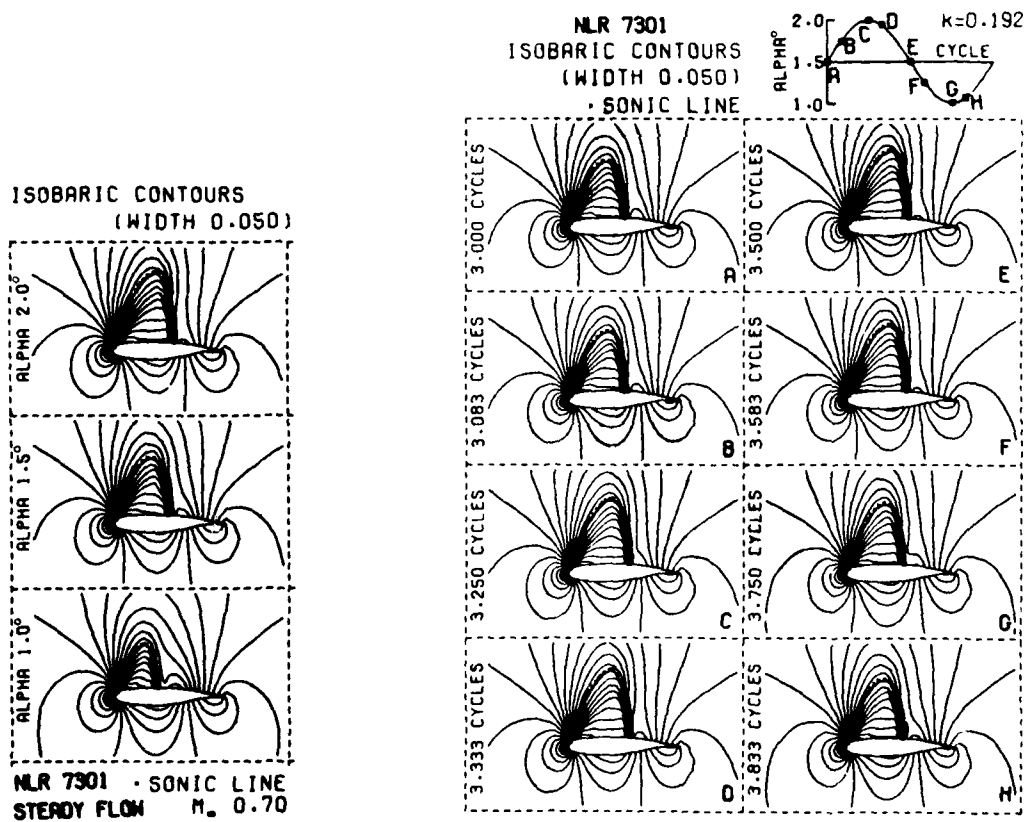


Fig 6-2 Steady isobaric contours

Fig 6-3 Unsteady isobaric contours

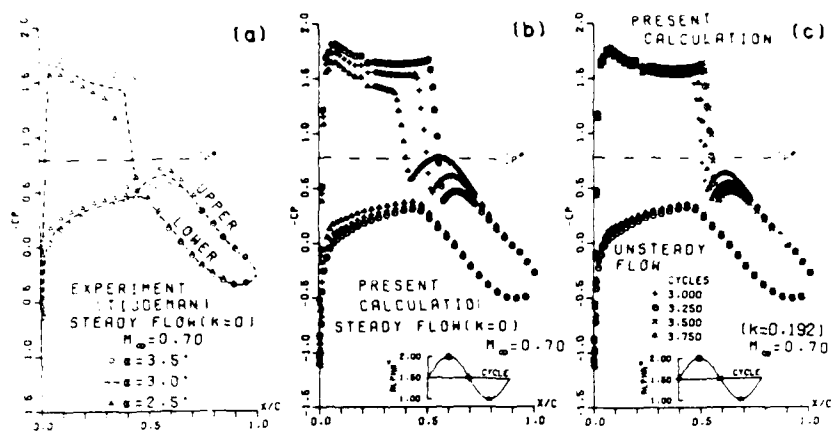


Fig 6-4 Steady and unsteady pressure coefficients

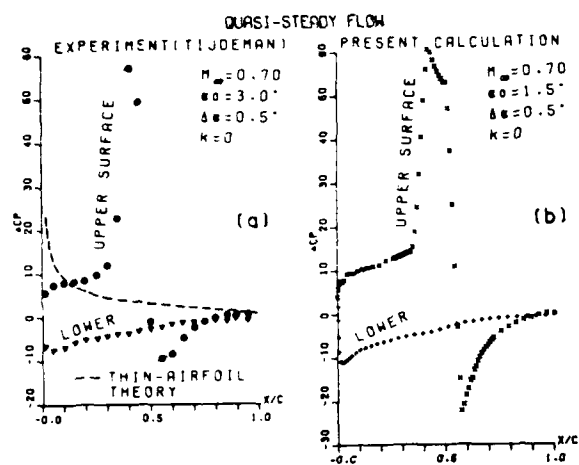


Fig 6-5 Comparison of quasi-steady pressure distributions

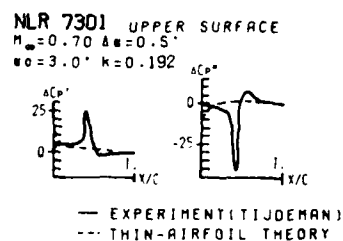


Fig 6-6 Experimental distributions of unsteady pressure

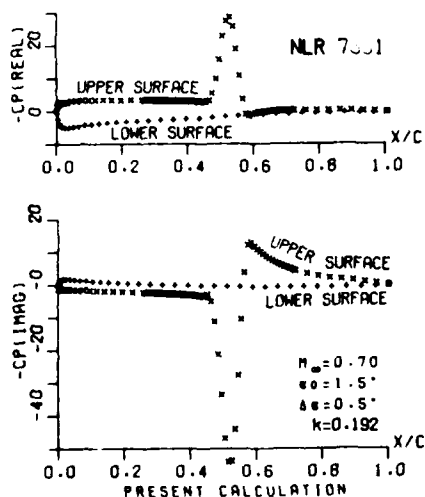


Fig 6-7 Unsteady pressure distribution by the present method of calculation

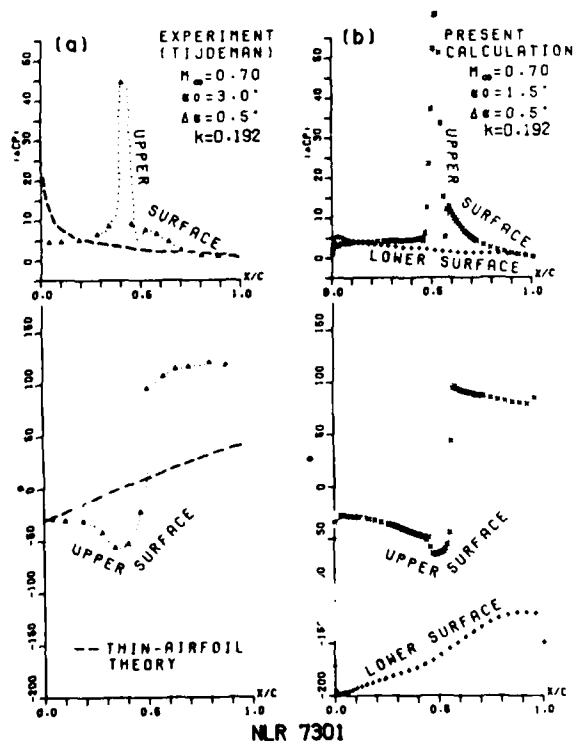


Fig 6-8 Comparison of unsteady pressure distributions

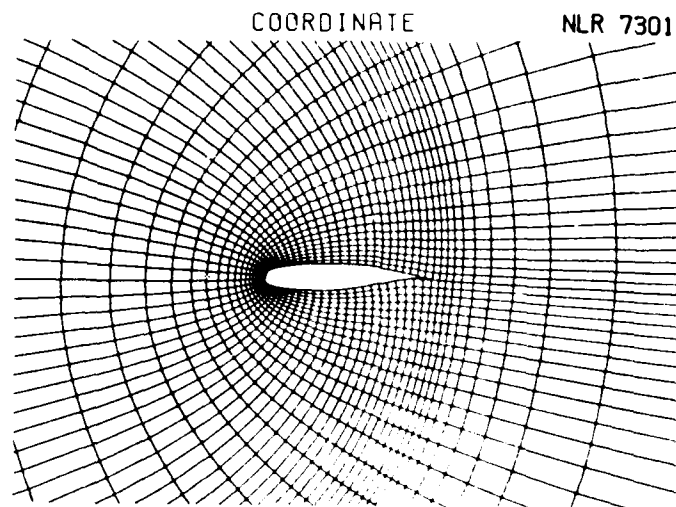


Fig 7-1 Grid image on the physical plane

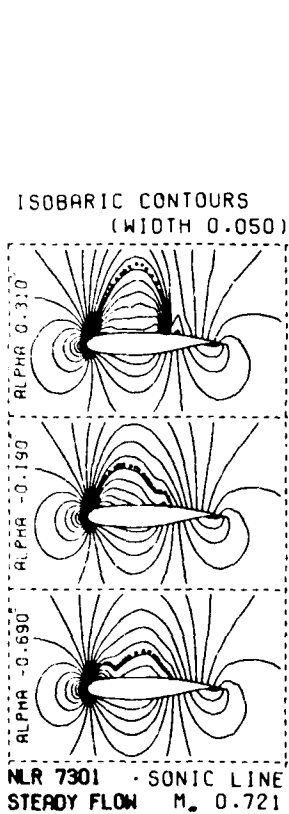


Fig 7-2 Steady isobaric contours

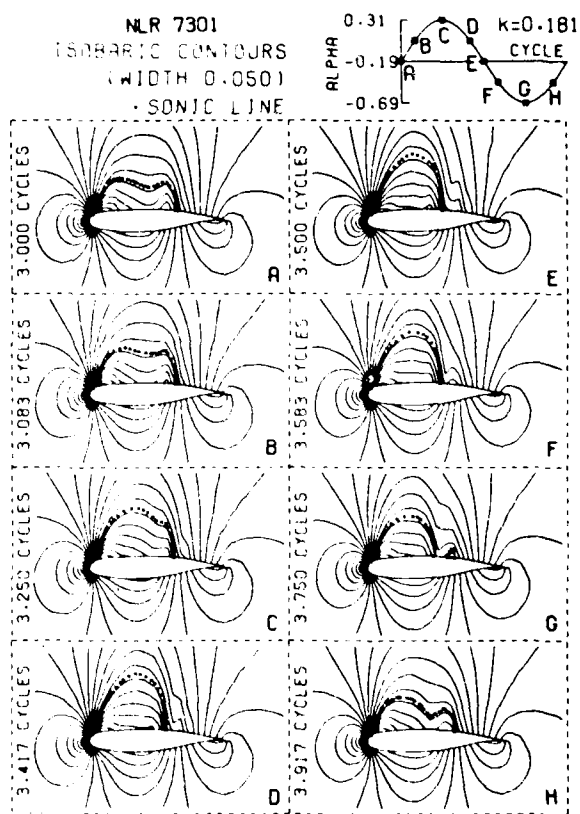


Fig 7-3 Unsteady isobaric contours

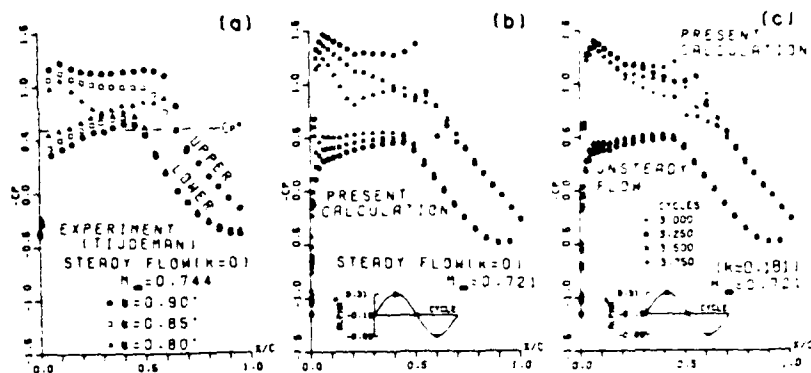


Fig 7-4 Steady and unsteady pressure coefficients

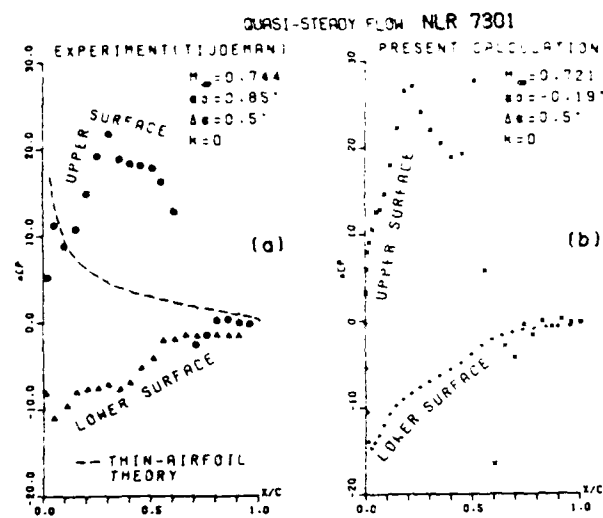


Fig 7-5 Comparison of quasi-steady pressure distributions

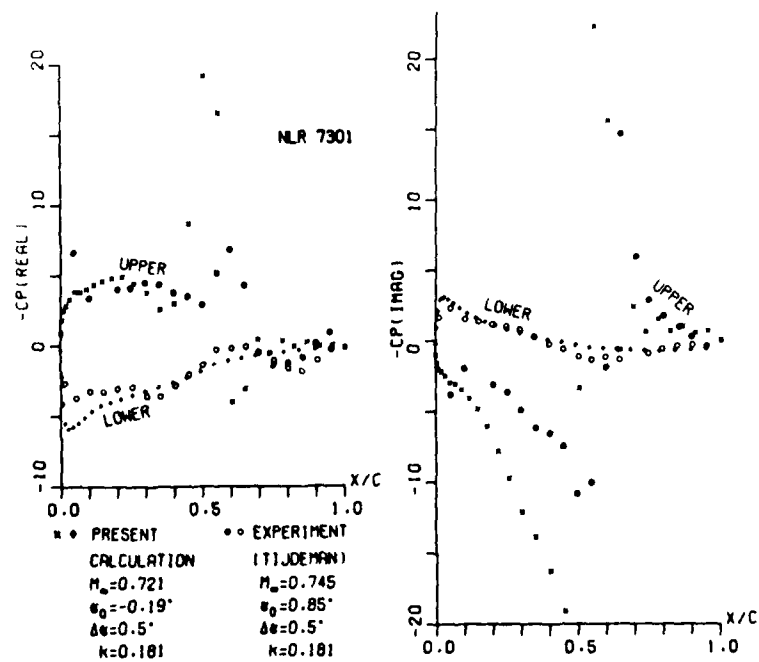


Fig 7-6 Comparison of unsteady pressure distributions

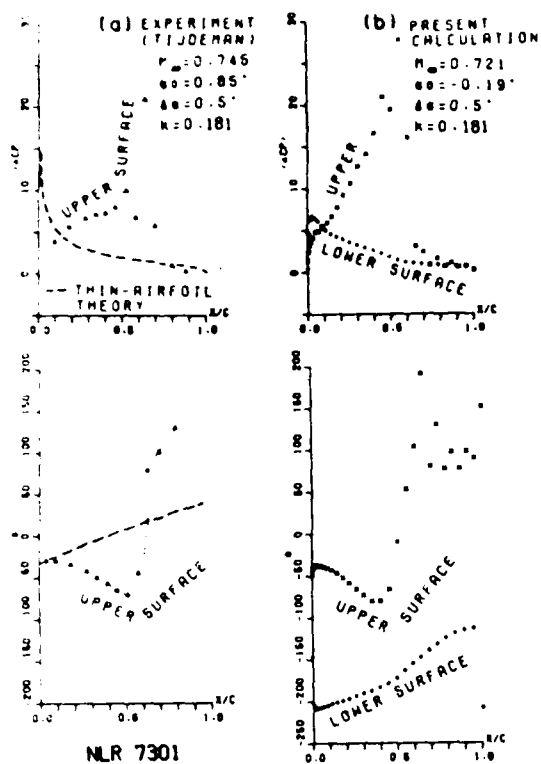


Fig 7-7 Comparison of unsteady pressure distributions

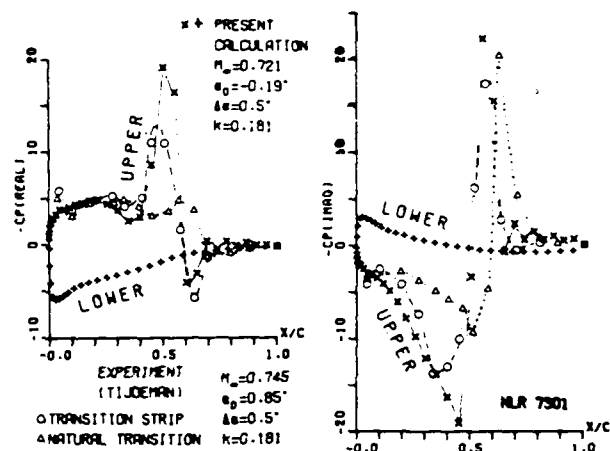


Fig 7-8 Comparison of unsteady pressure distributions

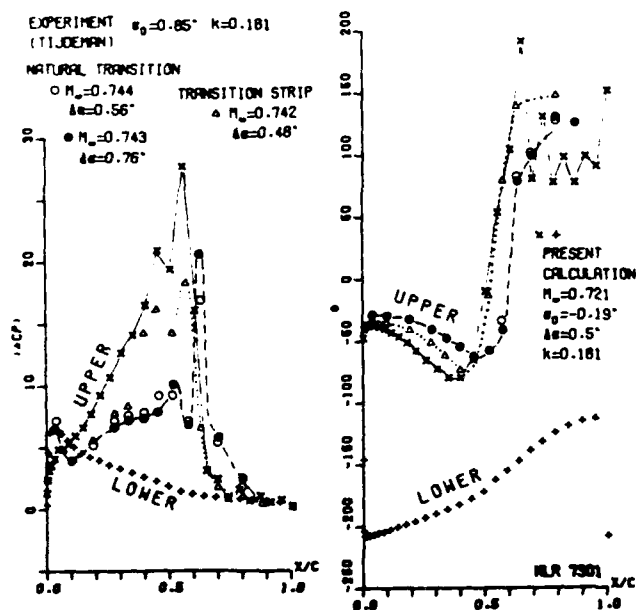


Fig 7-9 Comparison of unsteady pressure distributions

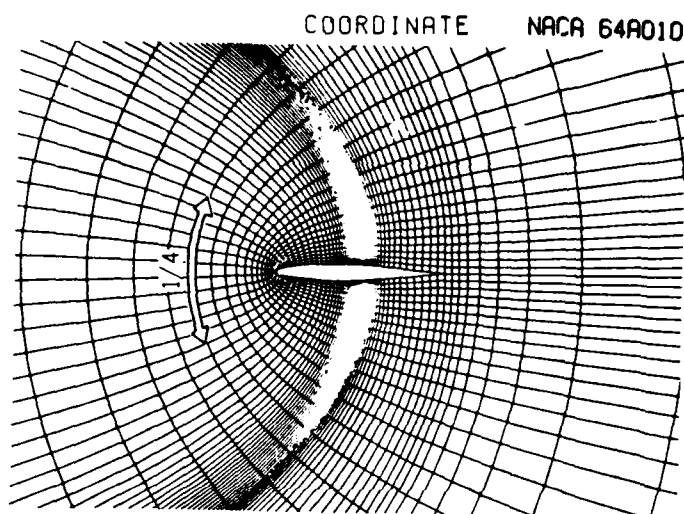


Fig 8-1 Grid image on the physical plane

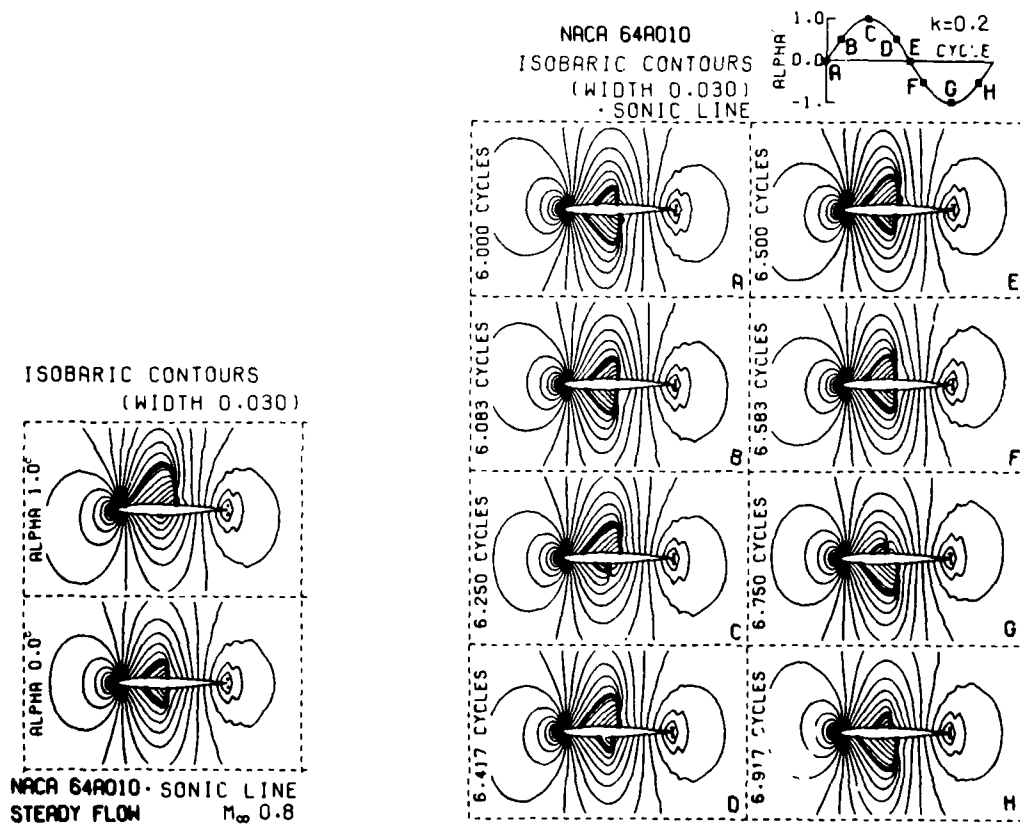


Fig 8-2 Steady isobaric contours

Fig 8-3 Unsteady isobaric contours

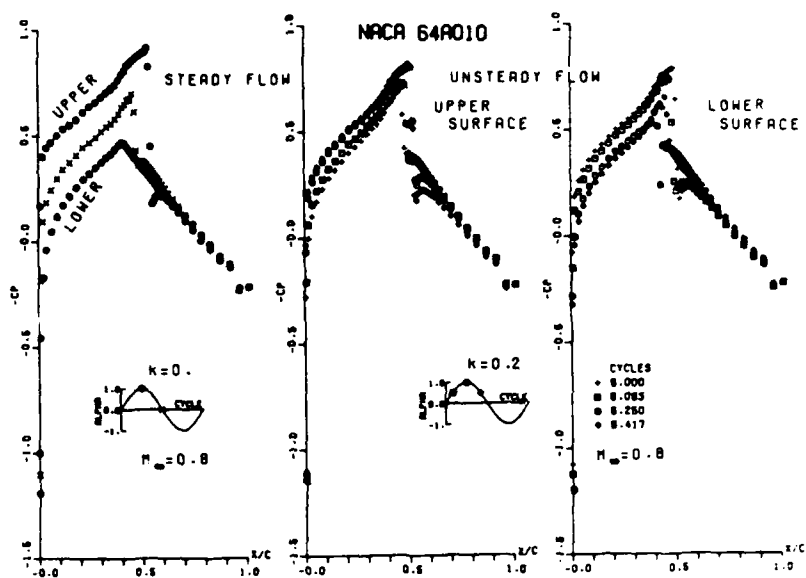


Fig 8-4 Steady and unsteady pressure coefficients obtained by the present method of calculation

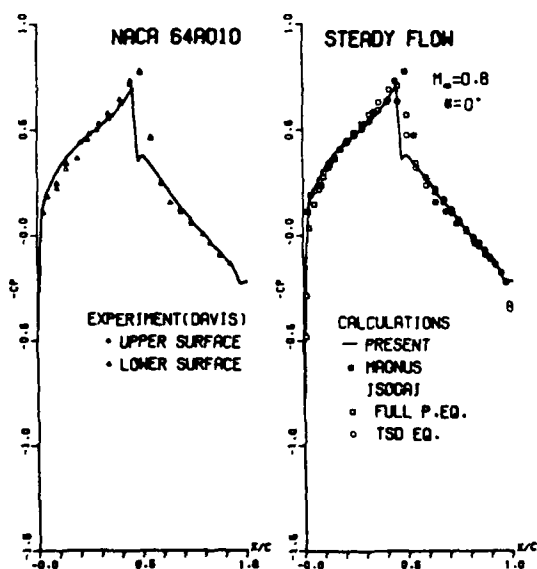


Fig 8-5 Comparison of steady pressure coefficients

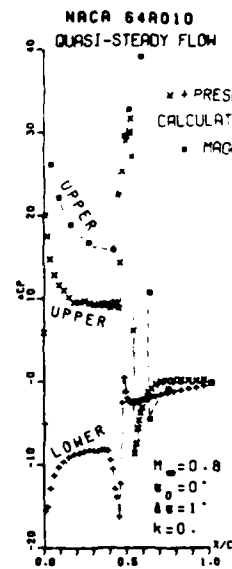


Fig 8-6 Comparison of quasi-steady pressure distributions

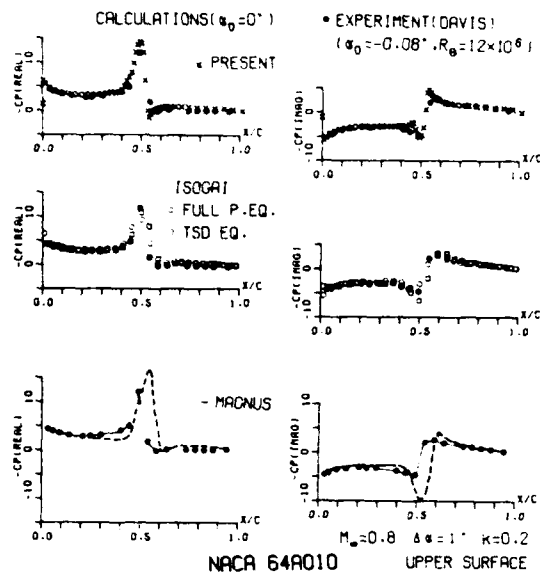


Fig 8-7 Comparison of unsteady pressure distributions

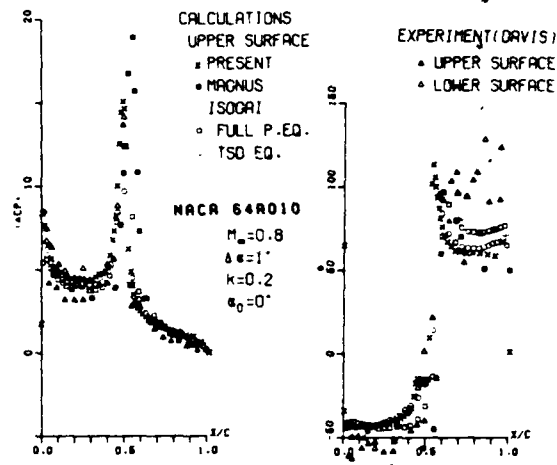


Fig 8-8 Comparison of unsteady pressure distributions

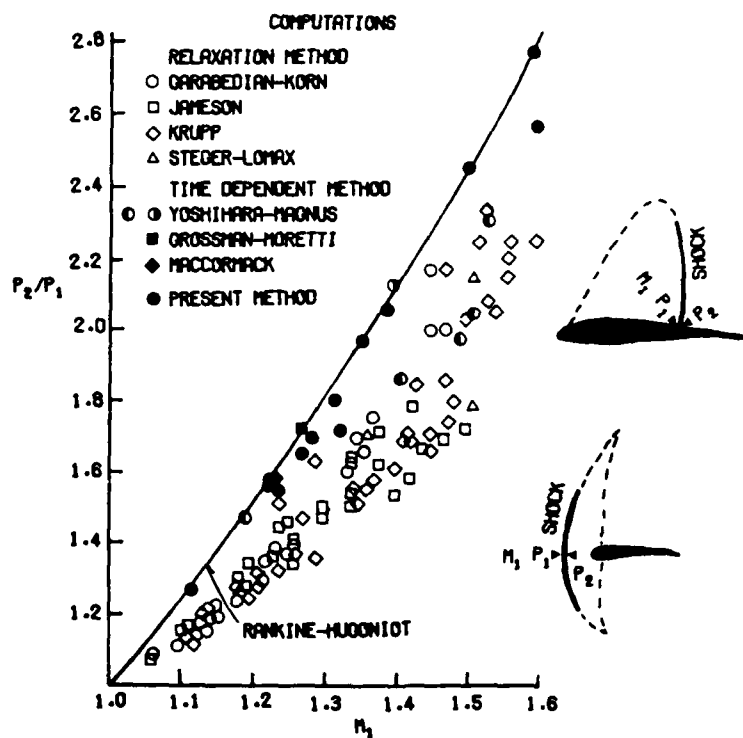


Fig 9 Deviation from the Rankine-Hugoniot relation

DAT
FILM
2-8